
ASTRO-H COOK BOOK

A First Step to ASTRO-H Spectral Analysis

Contents

Main Sections

0. ASTRO-H Spectroscopy.....	3
1. Hydrogen-Like Ion.....	4
Atomic Structure.....	4
Atomic Process.....	5
Overview of Atomic processes.....	7
2. Helium-Like Ion.....	8
Fine structure.....	8
He-like Plasma Diagnostics.....	9
Collisional plasmas.....	10
Ionizing and recombining plasmas.....	11
Photoionized plasma.....	11
Observing with Astro-H SXS.....	13
3. Multiple-Electron.....	14
Periodic table.....	14
Inner shell atomic process.....	19
Topic: Nomenclature for X-ray Astrophysics.....	20
4. Astrophysical Plasma.....	24
Various astrophysical plasma.....	24
Collisional Ionization Equilibrium (CIE).....	26
Photo ionization Equilibrium (PIE).....	27
Spectral Examples of CIE and PIE.....	28
Non-equilibrium ionization.....	31
5. Radiative Transfer.....	32
Absorption.....	32
Resonance scattering.....	33
Dust scattering.....	33
6. Line Width and Shift.....	34
Line profile and width.....	34
Line energy shift.....	35
Topic: Spectral signature hints and flowcharts, Spectral signature hints and flowchart..	36
Topic: ASTRO-H White Paper Science.....	37

Coffee break

Electron spin, relativistic effect and transition.....	6
3D Periodic Table?.....	16
'Aufbau' principle.....	17
Moseley's law.....	17
Importance of Preceise Energies for Lines.....	17
The names of 1s-np transitions.....	23
Plasma Codes and Spectral Fitting Packages.....	25
Turbulence expected in cluster of galaxies.....	34
Cosmic redshift seen in GRB aftergrow.....	35
Doppler shift by outflows in AGNs.....	35
White dwarf mass estimation by gravitational redshift	35
Traveling to AKIHABARA.....	42

Examples

Iron Lines from an X-ray Binary Centaurus X-3.....	40
--	----

ASTRO-H Spectroscopy

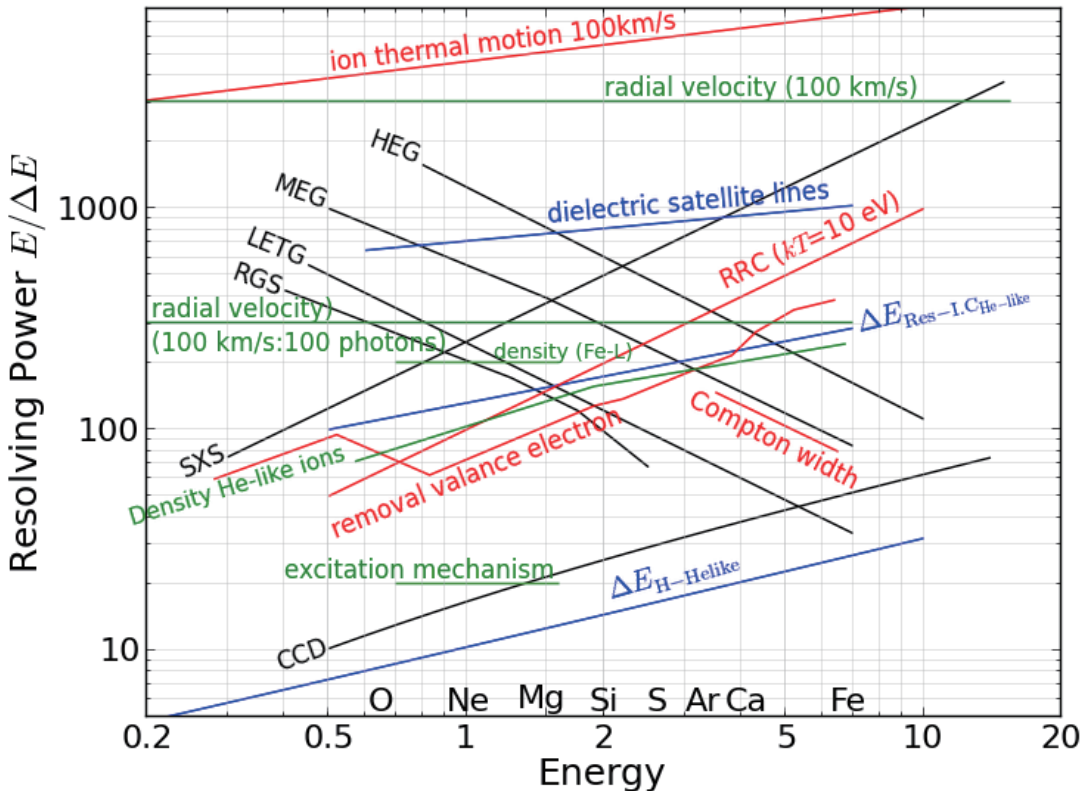


Figure 0.1: Spectral resolving power with different missions and instruments.
The original figure is from Frederik Paerels.

Our Universe is filled with a variety of forms of ionized plasma which accounts for most of our cosmic baryonic matter. Thermal X-ray radiation with atomic emission lines provides us valuable astrophysical plasma diagnoses to probe a wide range of astrophysics. Spectroscopy with a moderate energy resolution of about 300 eV ($R \sim E/\Delta E \sim 20$) has already enabled us to distinguish various atomic transitions from different charge states and/or principal quantum numbers. Diagnostics of emission lines, (e.g., iron K α and K β lines) have been useful tools to measure plasma temperatures.

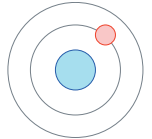
The ASTRO-H Soft X-ray Spectrometer (SXS) will reach the energy resolution of ~ 7 eV at 6 keV ($R \sim 800$). This resolution will provide us a way to distinguish atomic fine structures at the same quantum number labeled by the quantum angular momentum. Transition probabilities and intensities are determined by electron quantum states which are strongly affected by the conditions of the plasma condition such as ionization mechanisms, temperature, and density, . The line diagnostics is thus a more powerful probe into the astrophysical plasma.

This cookbook is prepared as a practical handbook for the ASTRO-H spectroscopy, mainly assuming fresh Ph.D students and young post docs. This cook book includes concise collections of up-to-date useful material including basic physical concepts, parameters, formulas, tables, and diagrams based on textbooks, papers, and reviews. Readers can refer to further materials from references in this cook book. This document is based on a long history of X-ray spectroscopy of Einstein, EXOSAT, ASCA, Chandra, XMM-Newton, and Suzaku. We hope to make this living document a practical and useful handbook during the ASTRO-H era.

Further reading...

1. ASTRO-H quick reference [[PDF](#)]
2. Takahashi T., et al., “The ASTRO-H X-ray Astronomy Satellite” (2014) SPIE [[PDF](#)]

Hydrogen-like Ion



Topic: Atomic structure of one electron system (Hydrogen-like ion or Bohr atom) and transitions between energy levels. The levels are described by principal quantum number $n=0, 1, 2, \dots$, and the atomic number Z . Our goal is to calculate the energy levels on the back of an envelope.

Atomic Structure

$$E_n = -1 \text{ Ry} \cdot \frac{Z^2}{n^2}$$

$1 \text{ Ry} = \frac{\alpha^2}{2} m_e c^2 = 13.60 \text{ eV}$
Rydberg unit (energy), Lyman edge

$\alpha = \frac{e^2}{\hbar c}$ (CGS) = $\frac{q_e^2}{4\pi\epsilon_0\hbar c}$ (SI) = $\frac{1}{137.0360}$
Fine structure constant

$$E\lambda = 12.39842 \text{ (keV} \cdot \text{\AA}) \quad 1 \text{ Ry} \rightarrow \lambda = 912 \text{ \AA} \quad \hbar c = 1973 \text{ (eV} \cdot \text{\AA}) \sim 2 \text{ (keV} \cdot \text{\AA})$$

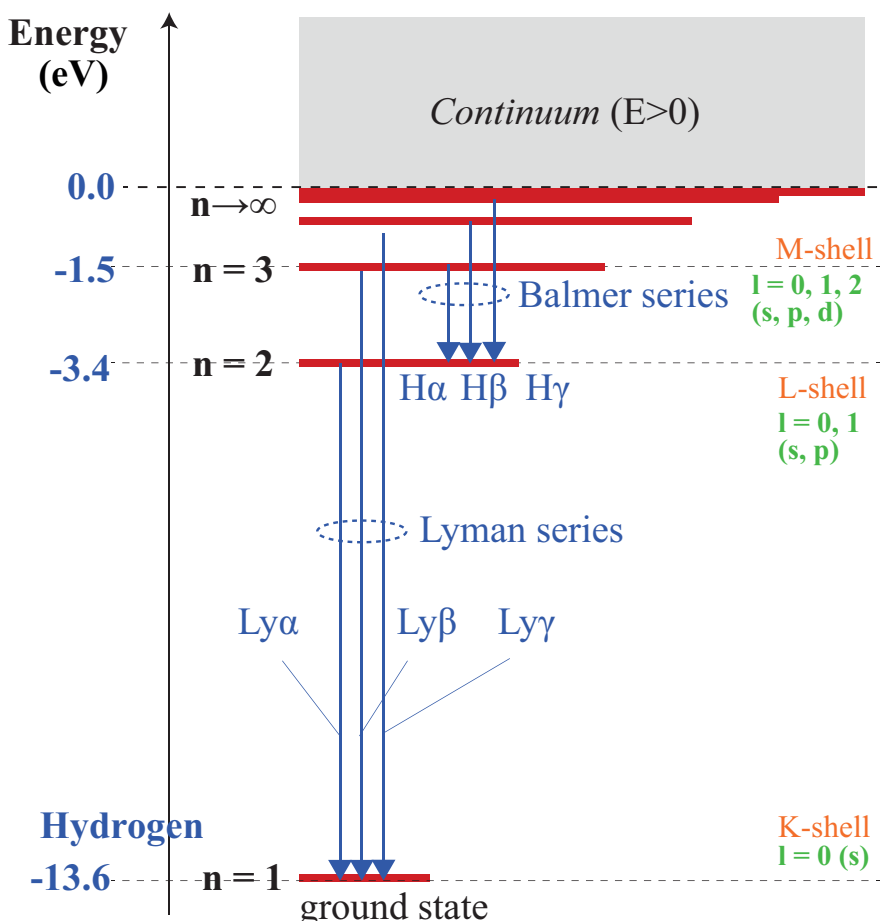
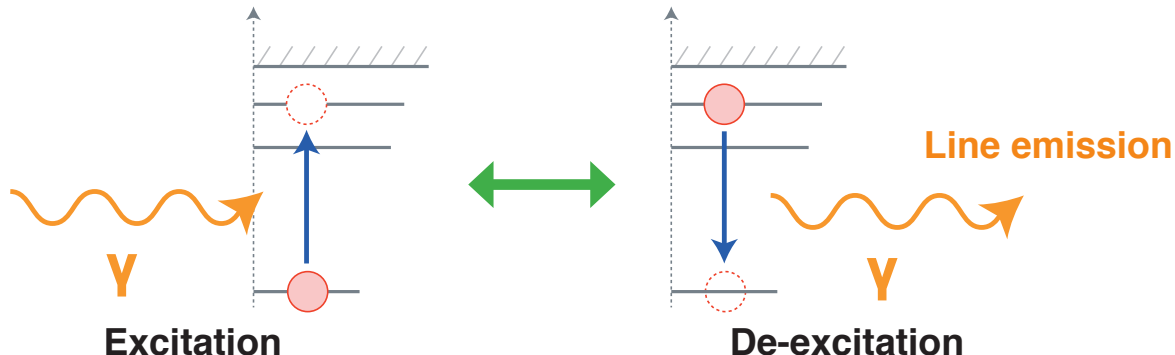


Figure 1.1: Atomic energy levels of the Hydrogen-like atom. Inner shell lines are denoted K α ($n=1$ to 2), K β ($n=1$ to 3), but not for H & He-like. Figure is modified from Astronomy methods : A Physical Approach to Astronomical observations (Cambridge Planetary science).

Atomic Process

Excitation & De-excitation (bound-bound)



$$E_{nm} \sim 1 \text{ Ry} \cdot Z^2 \left(\frac{1}{n^2} - \frac{1}{m^2} \right)$$

Photoexcitation \Leftrightarrow Radiative de-excitation
Collisional excitation \Leftrightarrow Collisional de-excitation

Table 1.1: Emissions/transitions from Hydrogen-like ion. See the details in AtomDB.

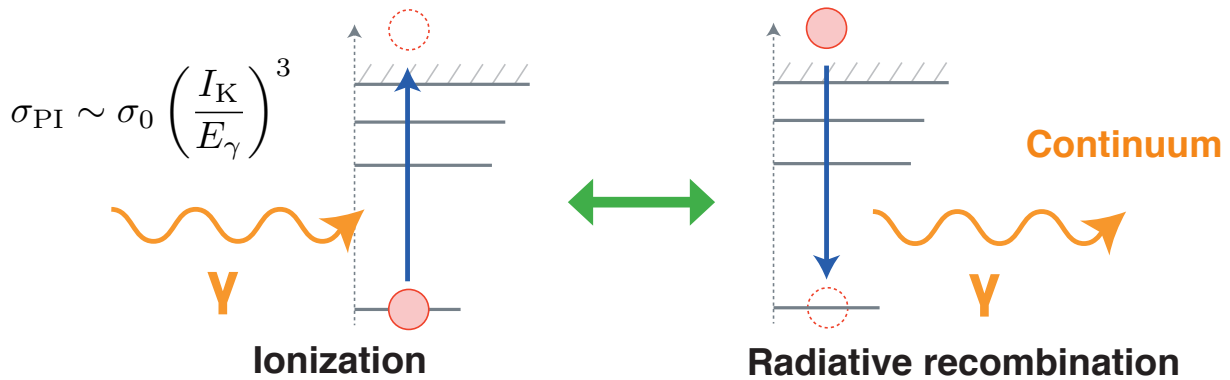
	Ly α_1 (n=2 \rightarrow 1)		Ly α_2 (n=2 \rightarrow 1)		K-edge (n= ∞ \rightarrow 1)	
	λ (Å)	E (keV)	λ (Å)	E (keV)	λ (Å)	E (keV)
O VIII	18.9671	0.65368	18.9725	0.65348	14.2280	0.871410
Ne X	12.1321	1.02195	12.1375	1.02150	9.10177	1.36220
Na XI	10.0232	1.23697	10.0286	1.23631	7.52011	1.64870
Mg XII	8.41920	1.47264	8.42461	1.47169	6.31714	1.96266
Al XIII	7.17091	1.72899	7.17632	1.72769	5.38093	2.30414
Si XIV	6.18043	2.00608	6.18584	2.00432	4.63808	2.67318
S XVI	4.72735	2.62270	4.73276	2.61970	3.54830	3.49419
Ar XVIII	3.73110	3.32299	3.73652	3.31817	2.80113	4.42622
Ca XX	3.01848	4.10750	3.02390	4.10014	2.26668	5.46986
Fe XXVI	1.778202	6.97316	1.78344	6.95197	1.33637	9.27769

Do you need transition energies? Searched in [NIST](#) or [AtomDB](#).

Further reading...

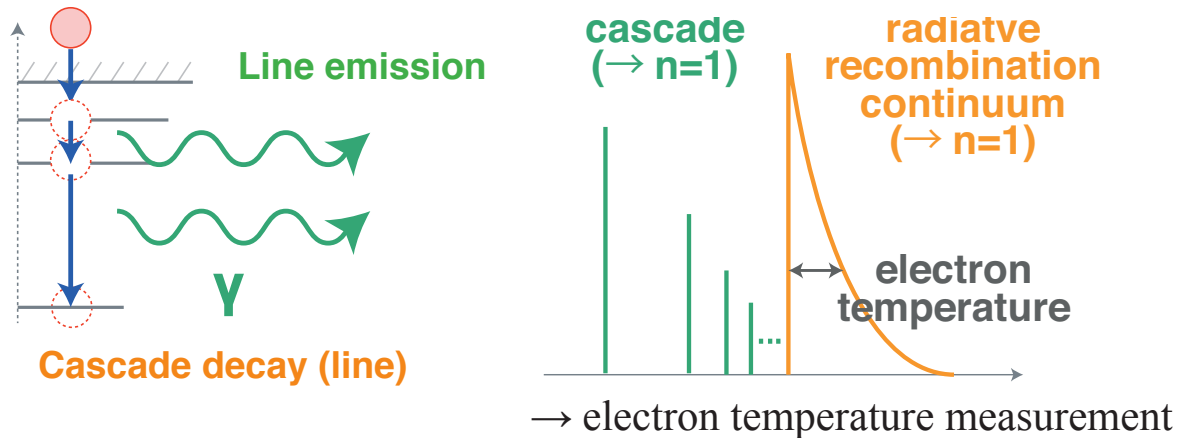
1. Herzberg, G., “Atomic Spectra and Atomic Structure” (1973) [\[amazon\]](#)
2. G. B. Rybicki & A. P. Lightman “Radiative Processes in Astrophysics” (1985) [\[amazon\]](#)
3. A. Thompson et al., “X-ray Data Booklet”, LBNL (2009) [\[link\]](#)
4. A. K. Pradhan and S. N. Nahar, “Atomic Astrophysics and Spectroscopy” (2011) [\[amazon\]](#)

Ionization & Recombination (bound-free)



Photoionization \Leftrightarrow Radiative recombination

Collisional ionization \Leftrightarrow Three body recombination



Coffee break: Electron spin, relativistic effect and transition

Energy levels are:

- also modified by orbital angular momentum number $l=0, 1, 2, \dots, n-1$ (s, p, d, f, g, h, respectively).
- For a purely radial electrostatic potential, E_n is independent of l .

Spin and relativistic effects:

- When electron spin is taken into account, there is another quantum number $s=\pm 1/2$ for one electron.
- Spin s and orbital angular momentum l are added as vectors to make total angular momentum quantum number $j=l\pm s$.
- Spin splits the l states in energies, ‘fine struc-

ture’ splitting (Dirac equation with L-S coupling)

- $\Delta E_{fs} = E_n \frac{\alpha^2 Z^2}{2n} \left(\frac{1}{j \pm 1/2} - \frac{3}{4n} \right)$
- Relativistic effects become important when $E_n/m_e c^2$ or heavier atoms $Z > 6$ (Carbon).

Transition speed:

- Transitions between energy levels: fastest transitions satisfy dipole selection rule .
- $\Delta l = 0, \Delta s = 0$
- Other transitions are slower by factors > 1000 .

Overview of Atomic processes

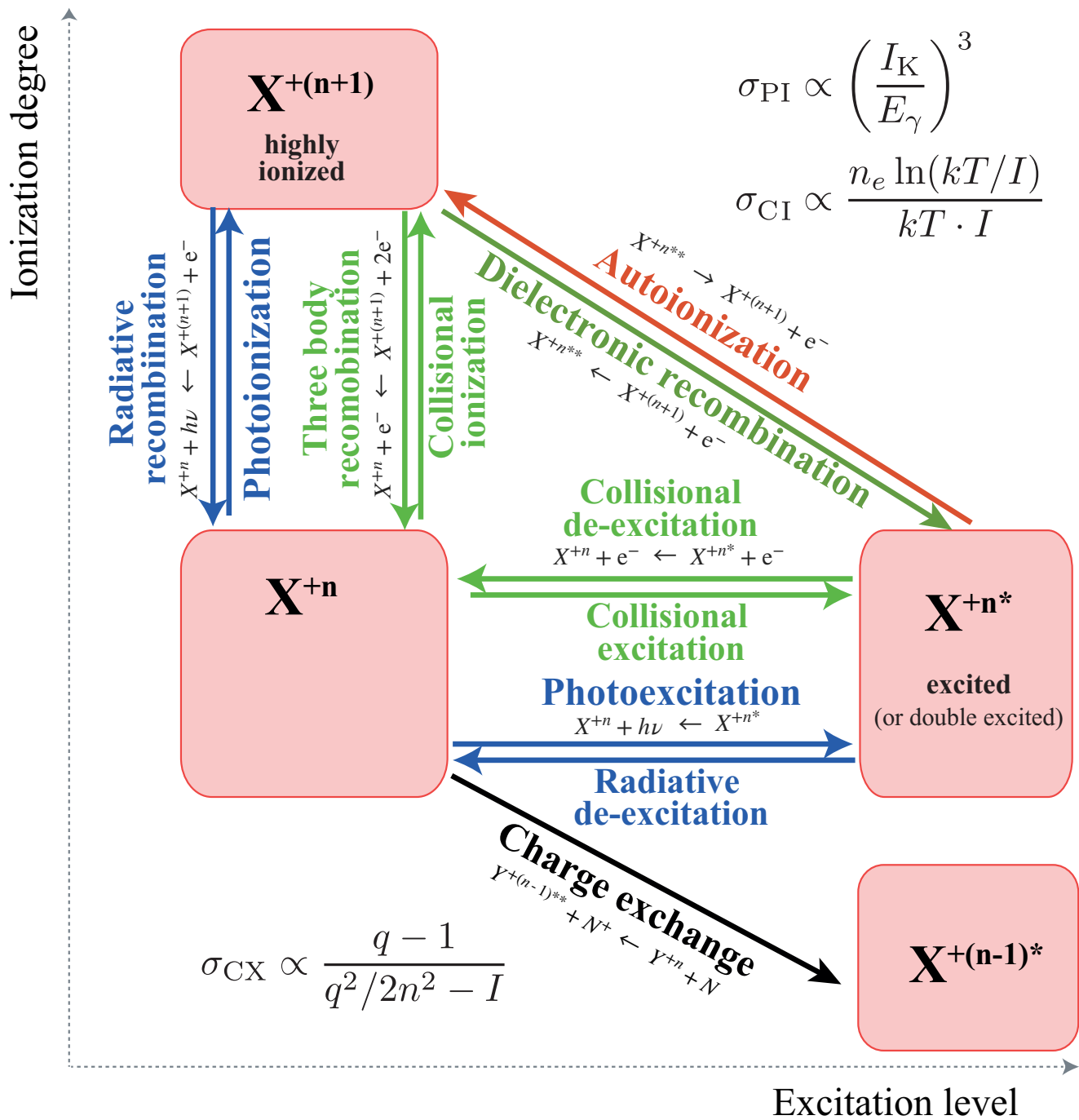
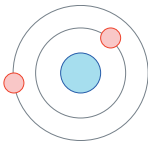


Figure 1.2: Schematic diagram of atomic processes

Further reading...

1. Kallman, T., and Palmeri, P., 2007, RvMP, 79, 79 [[ADS](#)]
2. Smith, R. K., and Brickhouse, N. S., 2014, AAMOP [[ADS](#)]
3. Kaastra, J. S., and Paerels, F. B. S., et al., 2008, SSRv, 134, 155 [[ADS](#)]
4. Porquet, D., Dubau, J., and Grosso, N., 2010, SSRv, 157 [[ADS](#)]
5. Arnaud, K., Smith., R. et al. "Handbook of X-ray Astronomy", Cambridge (2011) [[link](#)]

Helium-like Ion



Topic: Ions with 2 electron (“He-like”) exist over a wide range of plasma temperatures due to the large ionization potential difference between the 3-electron and 2-electron ions. The $n = 2 \rightarrow 1$ transition of these elements lies in the X-ray band, providing bright lines in the X-ray spectrum.

Fine Structure

The total spin and orbital angular momenta, denoted S and L , are vector sums of the individual electrons. $\vec{L} = \sum_i \vec{l}_i$ $\vec{S} = \sum_i \vec{s}_i$ $\vec{J} = \vec{L} + \vec{S}$

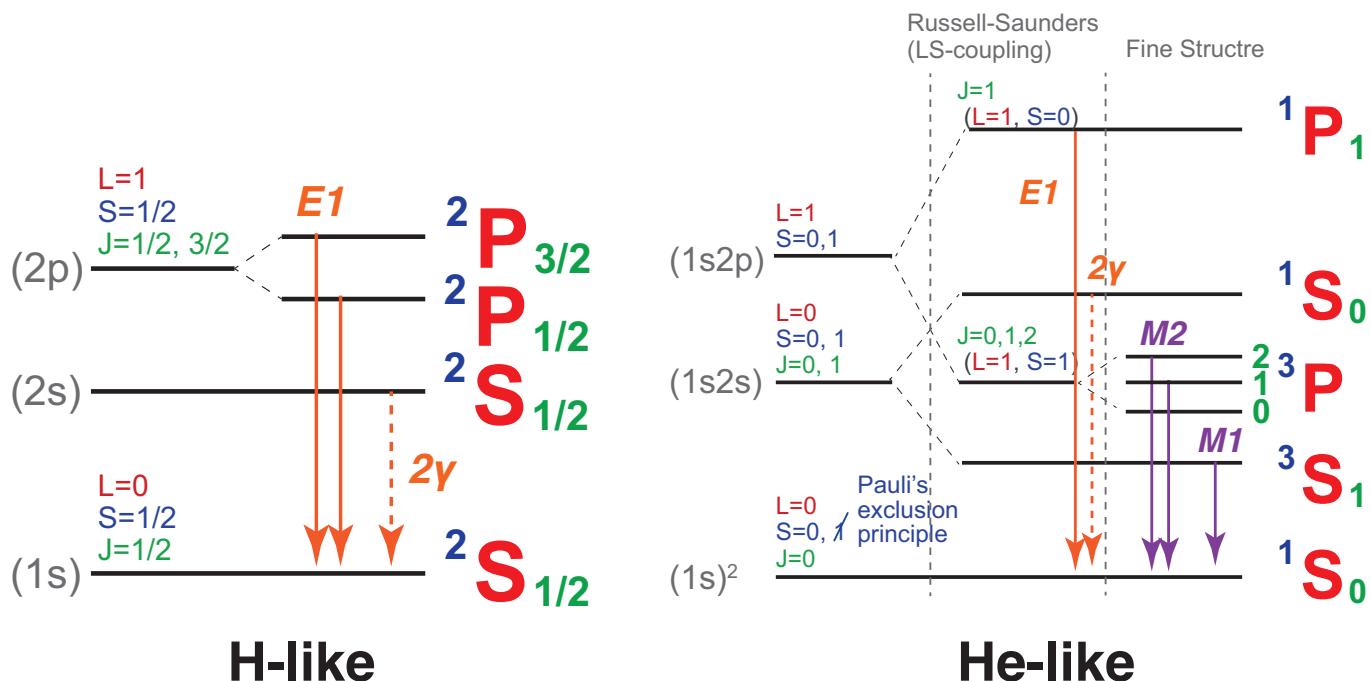
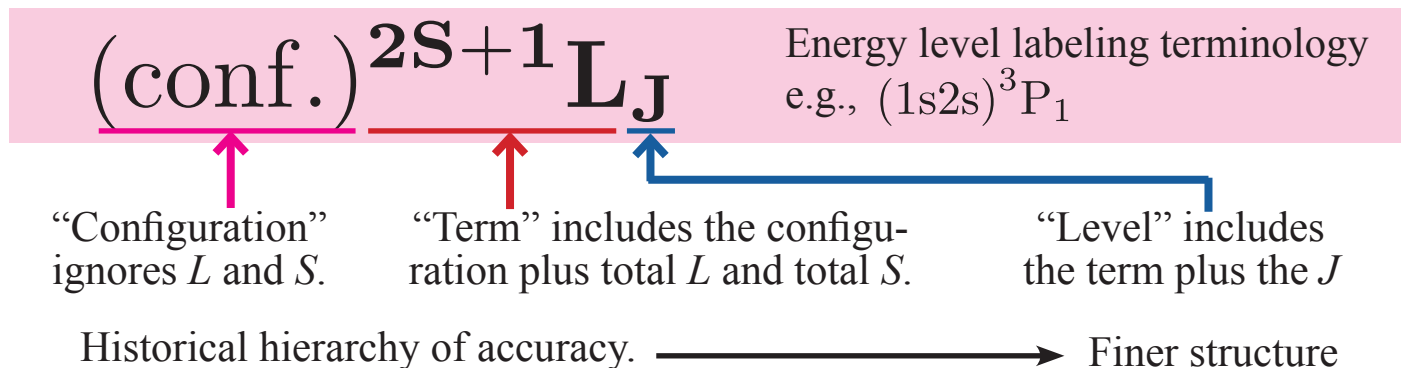


Figure 2.1: Schematic diagram of energy levels of H-like and He-like ions.

Selection rules

Initial and final states of permitted transition. Transitions which do not satitsfy these rules are not slow. ($J=0$ to $J=0$ is not allowed)

$$\Delta S = 0, \quad \Delta L = \pm 1, \quad \Delta J = 0, \pm 1$$

He-like Plasma Diagnostics

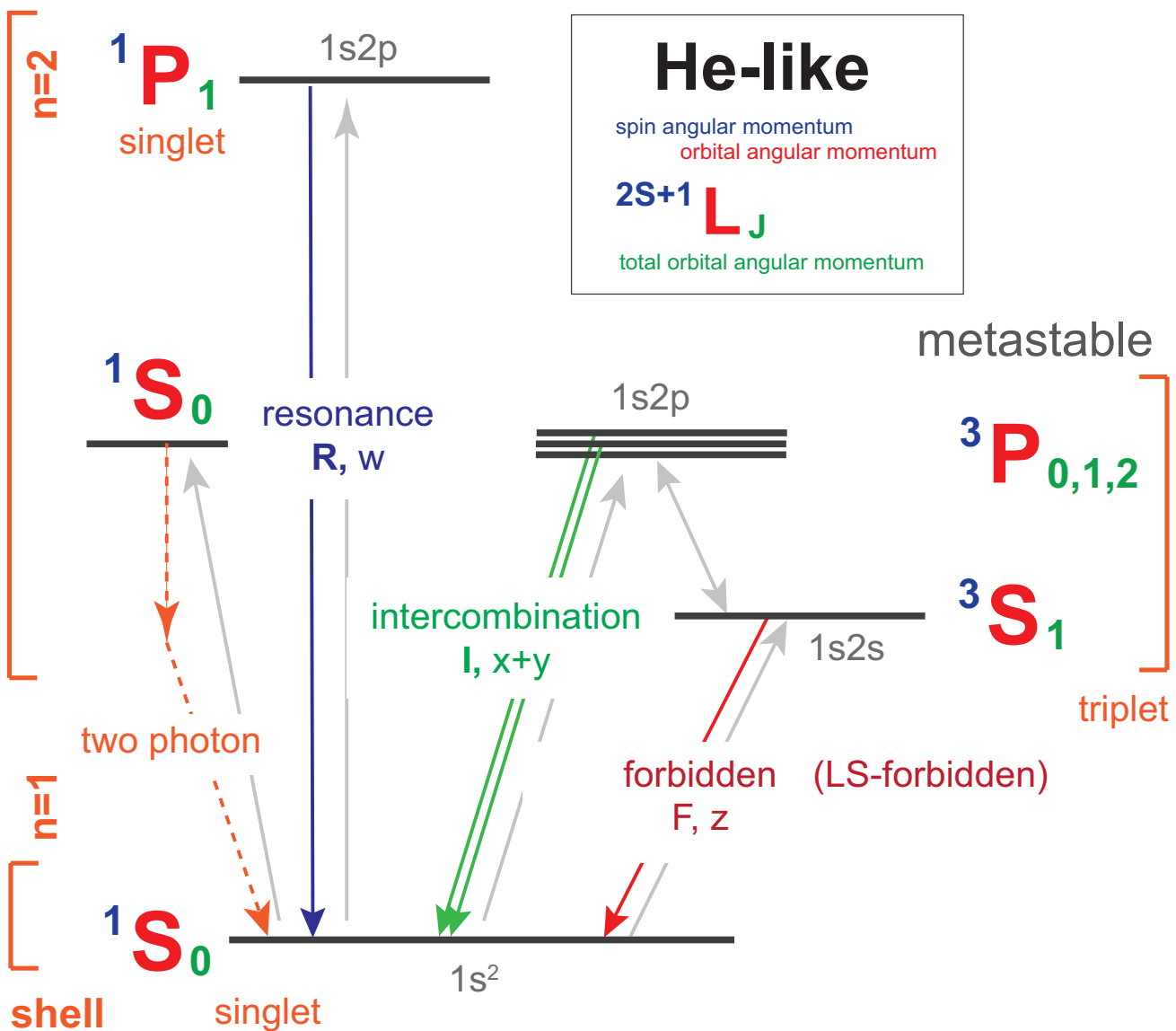


Figure 2.2: Schematic diagram of energy levels of He-like ions.

The 2 electrons system, shown in figure 2.2 has 4 lines: the resonance (R or w), forbidden (F or z) and 2 intercombination lines, (I, or x and y) (names from Gabriel & Jordan, 1969 [[link](#)]). The intercombination lines are often treated as one line, as their wavelengths are close enough to be unresolvable in most spectra. The He-like system has triplet ($S = 1$) and singlet ($S = 0$) spin systems. Transition rates within a spin system can be fast, transition rates between them are always slow. The w line is the dipole allowed transition from $^1P_1 \rightarrow \text{gnd}$, with a high transition rate.

The z line, from $^3S_1 \rightarrow \text{gnd}$, has a much lower transition rate; as this is the lowest energy level it form a metastable state, i.e. one with such low outgoing transition rates that a significant population can build up in it, acting almost as a second ground state. It is this metastable which gives the density and temperature sensitivity of the lines.

These lines are considered particularly important due to their clarity in the spectrum, and their origin from the same ion. This removes questions of relative elemental abundance, or even of the ion distribution from consideration, making interpretation easier.

Collisional Plasmas

Density Diagnostic, $R(\text{Ne})=z/(x+y)$:

At low densities, any population in the 3S_1 state has to decay to ground by the z line. The population in the $^3P_{1,2}$ levels has a fixed branching ratio between transitions to the ground and transition to the 3S_1 level, which in turn enhances the z line. As density increases, there are more and more collisions between electron and the ions, which are highly efficient at redistributing between different L states with small energy differences. At the critical density, N_{crit} , the collisional excitation rate, $N_e q^3 S_1 \rightarrow ^3 P_{1,2}$ (q is the collisional excitation rate coefficient) starts to dominate the radiation to ground, $A^3 S_1 \rightarrow \text{gnd}$. This means population from the 3S_1 metastable level excites to the $^3P_{1,2}$ levels then radiates to the ground, increasing the inter-

combination line and supressing the forbidden line.

Due to the different Z dependence of the ions, the critical density changes for each ion. An approximate form is:

$$N_{\text{crit}}(Z) = 6.75(Z - 1)^{11.44}(\text{cm}^{-3}) \quad (1)$$

Temperature Diagnostic, $G(\text{Te})=(x+y+z)/w$:

At low temperatures, the spin changing excitation rates (i.e. from the ground to the 3S and 3P states) are similar to those to the 1P states. As temperature rises, the excitation rate to the 1P state rises sharply, which those to the triplet states remain largely unchanged. This leads to an increase in the w line relative to the other lines, and a reduction in the G ratio.

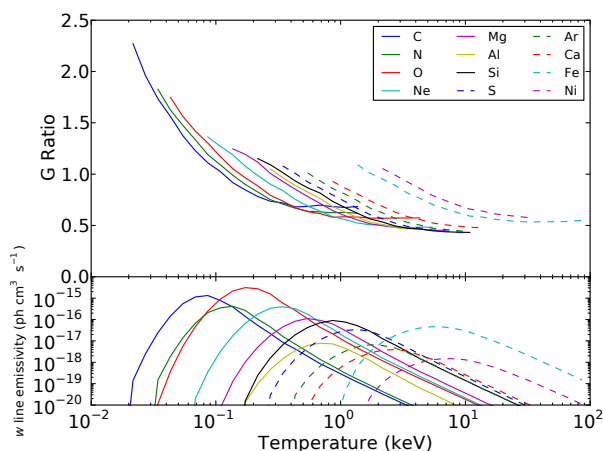
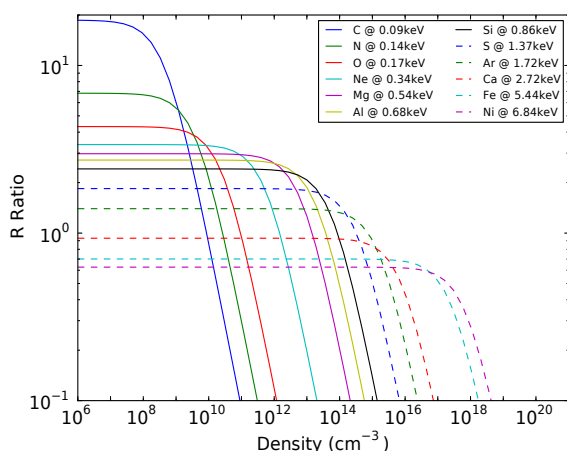


Figure 2.3: The R ratio (left panel) and G ratio (right panel) for a range of elements, as a function of electron density, at the temperature of their peak emissivity

Ionizing and Recombining Plasmas

Ionizing Plasma

When ionizing from a Li-like ion (ground state: $1s^22s$) to a He-like ion, the ionized ion preferentially either ends up in the ground state of He-like (if the $2s$ electron is removed) or a $1s2s$ state, either 1S_1 or 3S_1 . The decay from the 1S_1 is via a 2-photon process, and therefore doesn't lead to any lines. As a result, the signature of pure ionization is a very strong z line and negligible other lines.

In the case of a recombining plasma, the levels are populated statistically, leading to a much increased triplet level population. This in turn leads to a significant increase in the z line, typically about a factor of 4. See Figure 2.4.

A purely collisionally ionizing plasma is essen-

tially never seen — in a realistic ionizing scenario there will always be excitation from the ground state of the He-like ion as well as ionization from the Li-like ion. This is shown in the right panel of Figure 2.4, where the w line is not, in fact zero, though there is still significant enhancement of the z line.

Similarly, it is rare to see a purely recombining collisional plasma: recombination is fairly inefficient at producing lines compared to excitation, therefore a large H-like to He-like population ratio is required to be observed from the G ratio. Maintaining a large enough H-like/He-like population to provide significant recombination.

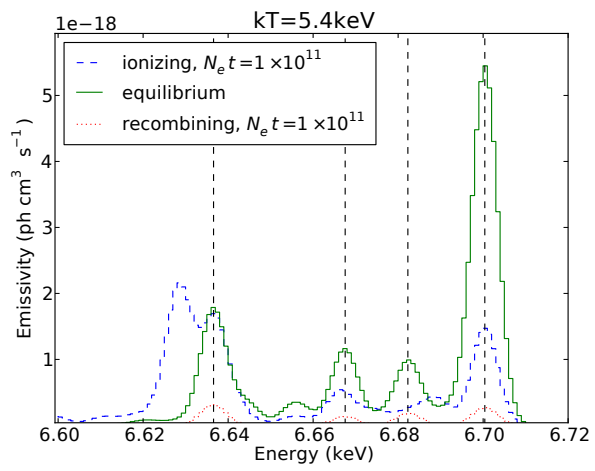
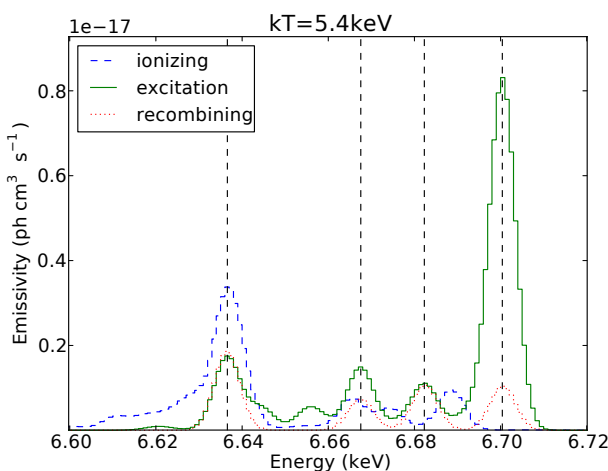


Figure 2.4: Left: The Iron He-like system for a purely ionizing, recombining and excitation driven plasma with $kT = 5.4$ keV. Right: The same, but for realistic recombining and ionizing plasmas with ionization age $10^{11} \text{ cm}^{-3} \text{ s}$. Both folded through a 7 eV SXS response.

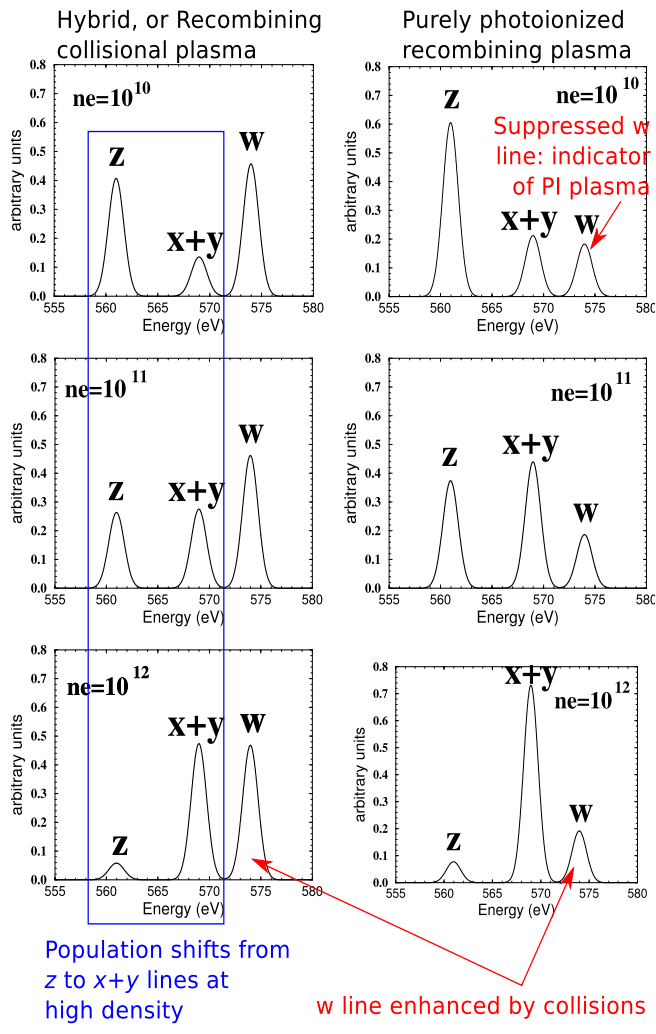
Photoionized Plasmas

Photoionization Diagnostic

Unlike in the case of a collisional plasma, in a photoionized plasma the excited levels of an ion are populated almost exclusively by recombination. Therefore the pure recombination process outlined above does happen. This increases the G ratio over the expected value in collisional equilibrium. So a G ratio which is larger than the range shown in Figure 2.3 (right) implies that recombination is driving the population of the He-like ions can be used as a strong indicator of a photoionized plasma. If there

is a significant w line, the plasma has at least some collisional processes occurring in it and it is not purely photoionized.

At higher temperatures, and with sufficient density, excitation from the ground state of the He-like ion can happen even in photo-ionized plasma, leading to a hybrid plasma. These are harder to diagnose but still have a slightly elevated G ratio. See Porquet & Dubau (2000) [[link](#)] for more.



R ratio in photoionized plasma

In a purely photoionized plasma, relatively cold electrons can still drive the collisional redistribution between the triplet states even when there is insufficient energy to excite the resonance line from the ground state. Therefore the R ratio remains a strong density diagnostic. It is complicated, however, by the need to account for several analyze several layers of data can become relevant as with the collisional plasma case. Therefore the R ratio can still be a density diagnostic, although the ratio at low density becomes a function of temperature, as the recombination processes of DR and RR populate the levels slightly differently (see Figure 2.6). density, excitation from the ground state of the He-like ion can happen even in photo-ionized plasma, leading to a hybrid plasma. These are harder to diagnose but still have a slightly elevated G ratio. See Porquet & Dubau (2000) [[link](#)] for more.

Figure 2.5: The He-like O spectrum for a purely photoionized plasma (right) and a partially photoionized, or hybrid, plasma (left), which is the same spectrally as a recombining collisionally ionized plasma. Shown at a range of different densities. Modified figure from Porquet & Dubau (2000) [[link](#)].

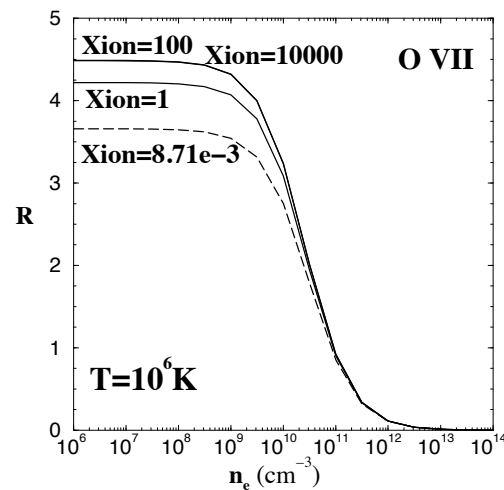
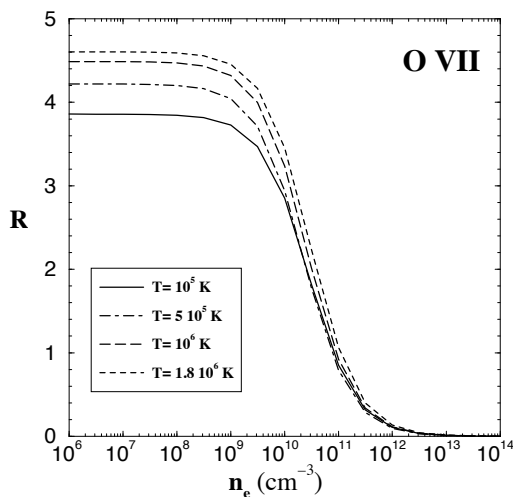


Figure 2.6: Left: The R ratio as a function of temperature in a purely photoionized plasma, with all levels populated by recombination and cascade from the H-like state. Right: In a hybrid plasma (partially photo-ionized, partially collisional) the R ratio depends on the Xion, the H-like to He-like ion population ratio. High values are a completely PI recombining plasma, low values include excitation from the ground by collisional excitation. From Porquet & Dubau (2000) [[link](#)].

Observing with Astro-H SXS

The energy resolution of the SXS is not sufficient to resolve all the details of the He-like system for lighter ions. Figure 2.7 shows the complex for collisionally ionized plasmas, with the w,x,y and z lines marked. This assumes a 10eV response for the SXS. For the Fe complex, the lines can be seen clearly. However for several of the lighter ions, there is overlap with other lines or insufficient resolution to distinguish lines in, for example, the G ratio. This does not mean the lines are useless, but great care is required to analyze them.

In a purely photoionized plasma, upper levels of the He-like ion are entirely populated by recombination from the H-like ion and subsequent cascade. The levels are populated according to their statistical weight, which leads to a factor of 4 increase in the triplet state populations compared with the singlet. This in turn increases the G ratio. So a G ratio which is larger than the range shown in 2 implies that recombination is driving the population of the He-like ions: this means either a strongly

recombining collisional plasma (rare, but possible) or a photoionized plasma.

At higher temperatures, and with sufficient density, excitation from the ground state of the He-like ion can happen even in photo-ionized plasma, leading to a hybrid plasma. These are harder to diagnose but still have a slightly elevated G ratio. See Porquet & Dubau (2000) [[link](#)] for more.

In conclusion, the relative intensity of the resonance w line, compared to the forbidden z and the intercombination (x + y) lines, contains informations about the ionization processes that occur: a weak w line compared to the z or the (x + y) lines corresponds to a pure photoionized plasma. It leads to a ratio of $G = (z+x+y)/w * 4$. On the contrary a strong w line corresponds to a hybrid plasma (or even a collisional plasma), where collisional processes are not negligible and may even dominate (see Sect. 3.3.2). In this case, w is at least as intense as the z or x + y lines.

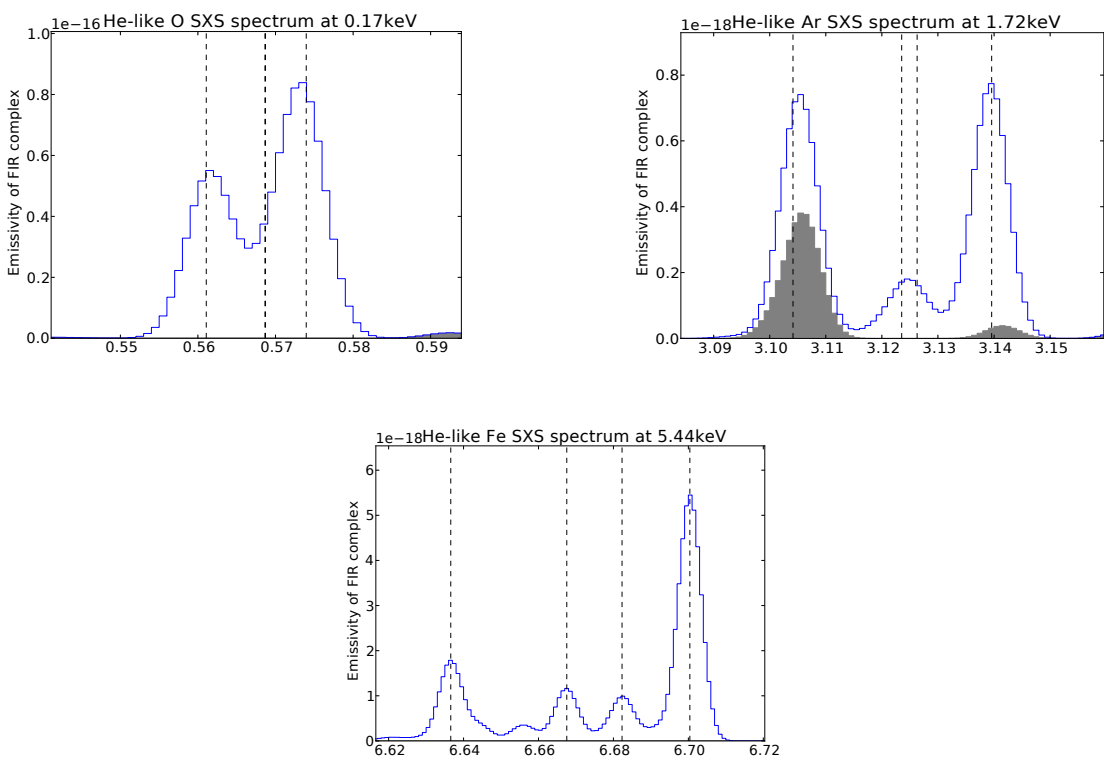
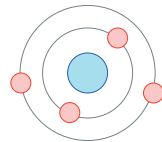


Figure 2.7: Collisionally ionized He-like triplets for O, Ar and Fe. In O, the intercombination lines are blended with the resonance line and are hard to distinguish. In Ar, there is significant blending with the Ca lines (denoted by shaded area). For Fe, all four lines can be resolved. The vertical dashed lines mark the w,x,y and z lines.

Multiple-electron



Topic: Multiple-electron atoms provide more physical processes and useful diagnostics (such as inner shell atomic processes) than single (Hydrogen-like) or two (Helium-like) electron systems. This chapter will be further updated in the next revisions.

Periodic table

Pauli exclusion principle: Two identical fermions cannot occupy the same quantum state simultaneously.

n: principal quantum number, $n = 1, 2, 3, \dots$

l: azimuthal quantum number $l = 0, 1, 2, \dots, n-1$

(*s*: sharp, *p*: principal, *d*: diffuse, *f*: fundamental)

m: magnetic quantum number, $m = 0, +1, \dots, +(l-1), -1$

s: spin projection quantum number, $s = -1/2, 1/2$

For the principal quantum number of *n*, the total number of the states is
 $\text{Sum}(l=0, n-1) [2*(2l+1)] = 2n^2 (2, 8, 18, \dots)$

So, why the 3rd row in the periodic table has only 8 elements?

Periodic table of Elements

1 IA	1 H Hydrogen 1.00794	2 IIA	4 Be Beryllium 9.012182	13 IIIA	5 B Boron 10.811	14 IVA	6 C Carbon 12.0107	15 VA	7 N Nitrogen 14.00674	16 VI	8 O Oxygen 16.9994	17 VIIA	9 F Fluorine 18.9984032	10 Ne Neon 20.1797	18 VIII	2 He Helium 4.0022602					
A Li Lithium 6.941	B Na Sodium 22.989770	Mg Magnesium 24.3050	C K Potassium 39.0983	Ca Calcium 40.078	Sc Scandium 44.959610	Ti Titanium 47.867	V Vanadium 50.9415	Cr Chromium 51.9961	Mn Manganese 54.938049	Fe Iron 55.8457	Co Cobalt 58.933200	Ni Nickel 58.6934	Cu Copper 63.546	Zn Zinc 65.409	Al Aluminum 26.98153	Si Silicon 28.0655	P Phosphorus 30.973761	Sulfur 32.066	Cl Chlorine 35.453	Ar Argon 39.948	
B Rb Rubidium 87.62	Sr Strontium 87.62	Yttrium 88.90685	Zr Zirconium 91.224	Nb Niobium 92.90638	Mo Molybdenum 95.94	Tc Technetium (97)	Ru Ruthenium 101.07	Rh Rhodium 102.90550	Pd Palladium 106.42	Ag Silver 107.6862	Cd Cadmium 112.411	In Indium 114.818	Ga Gallium 69.723	Ge Germanium 72.64	As Arsenic 74.92160	Selenium 78.96	Br Bromine 79.904	Kr Krypton 83.978			
C Cs Cesium 132.90545	Ba Barium 137.327	Hf Hafnium 178.49	Ta Tantalum 180.9479	W Tungsten 183.84	Re Rhenium 186.207	Os Osmium 190.23	Ir Iridium 192.217	Pt Platinum 195.078	Au Gold 196.56655	Hg Mercury 200.59	Tl Thallium 204.3833	In Tin 188.710	Sn Antimony 121.760	Te Tellurium 127.60	Iodine 126.9447	Xe Xenon 131.203	Rn Radon (222)				
F Fr Francium (223)	Ra Radium (226)	89-103	104 Rutherfordium (261)	Db Dubnium (262)	Sg Seaborgium (266)	Bh Bhabham (264)	Hs Hassium (269)	Mt Mendelevium (268)	Ds Dembinski (271)	Rg Roentgenium (285)	Uut Uutonium (284)	Pb Lead (207)	Bi Bismuth (209)	Po Polonium (210)	At Astatine (210)	Uus Ununseptium (292)	Uuo Ununoctium (unknown)				
57 La Lanthanum 138.9055	58 Ce Cerium 140.116	59 Pr Praseodymium 140.90765	60 Nd Neodymium 144.24	57 La Lanthanum 138.9055	58 Ce Cerium 140.116	59 Pr Praseodymium 140.90765	60 Nd Neodymium 144.24	57 La Lanthanum 138.9055	58 Ce Cerium 140.116	59 Pr Praseodymium 140.90765	60 Nd Neodymium 144.24	61 Sm Samarium 150.36	62 Eu Europium 151.964	63 Gd Gadolinium 157.25	64 Tb Terbium 158.92534	65 Dy Dysprosium 162.500	66 Ho Holmium 164.93032	67 Er Erbium 167.259	68 Tm Thulium 168.93421	69 Yb Ytterbium 173.04	70 Lu Lutetium 174.967
89 Ac Actinium (227)	90 Th Thorium 232.0381	90 Pa Protactinium 231.03588	92 U Uranium 238.02891	93 Np Neptunium (237)	94 Pu Plutonium (244)	95 Am Americium (243)	96 Cm Curium (247)	97 Bk Berkelium (247)	98 Cf Californium (251)	99 Es Einsteinium (252)	100 Fm Fermium (257)	101 Md Mendelevium (258)	102 No Nobelium (259)	102 Lr Lawrencium (262)	Br Liquid	c Solid	H Gas	Tc Sint			

This is because 4s is more stable than 3d. (ns is more stable than $(n-1)d$.)
 See the atomic configuration below.

Electron orbit

Table: atomic configuration (H to Zn)

	Z	K	L	M	N	Ground Level			
		1s	2s	2p	3s	3p	3d	4s	
H	1	1							$^2S_{1/2}$
He	2	2							1S_0
Li	3	2	1						$^2S_{1/2}$
Be	4	2	2						1S_0
B	5	2	2	1					$^2P_{1/2}$
C	6	2	2	2					3P_0
N	7	2	2	3					$^4S_{3/2}$
O	8	2	2	4					3P_1
F	9	2	2	5					$^2P_{3/2}$
Ne	10	2	2	6					1S_0
Na	11	2	2	6	1				$^2S_{1/2}$
Mg	12	2	2	6	2				1S_0
Al	13	2	2	6	2	1			$^2P_{1/2}$
Si	14	2	2	6	2	2			3P_0
P	15	2	2	6	2	3			$^4S_{3/2}$
S	16	2	2	6	2	4			3P_2
Cl	17	2	2	6	2	5			$^2P_{3/2}$
Ar	18	2	2	6	2	6			1S_0
K	19	2	2	6	2	6		1	$^2S_{1/2}$
Ca	20	2	2	6	2	6		2	1S_0
Sc	21	2	2	6	2	6	1	2	$^2D_{3/2}$
Ti	22	2	2	6	2	6	2	2	3F_2
V	23	2	2	6	2	6	3	2	$^4F_{3/2}$
Cr	24	2	2	6	2	6	5	1	7S_3
Mn	25	2	2	6	2	6	5	2	$^6S_{5/2}$
Fe	26	2	2	6	2	6	6	2	5D_4
Co	27	2	2	6	2	6	7	2	$^4F_{9/2}$
Ni	28	2	2	6	2	6	8	2	3F_4
Cu	29	2	2	6	2	6	10	1	$^2S_{1/2}$
Zn	30	2	2	6	2	6	10	2	1S_0

- Inner shell lines are denoted K α (n=1 to 2), K β (n=1 to 3), but not for H & He-like ions. (TK)

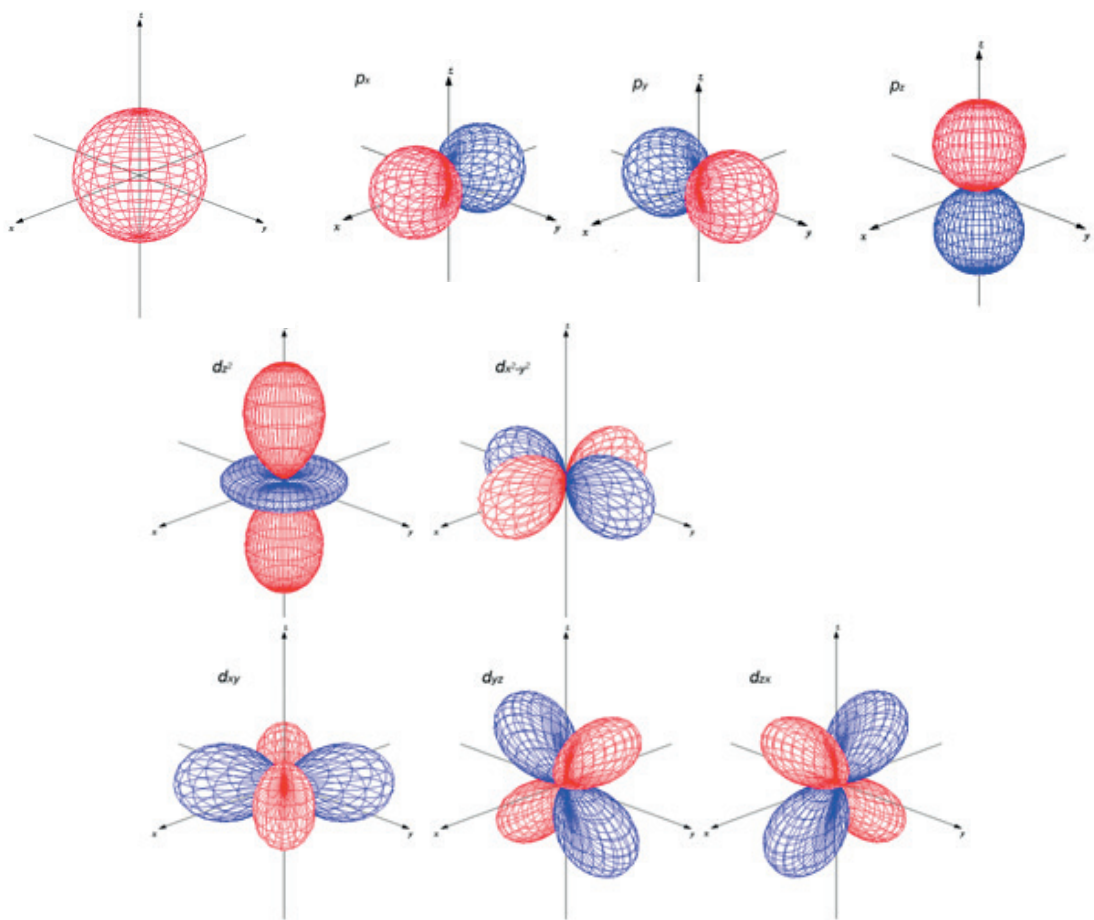
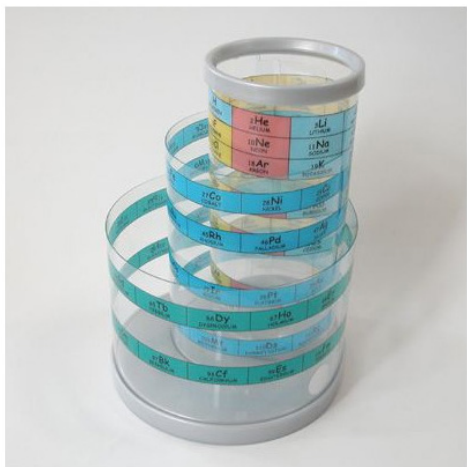


Figure X.X: Orbital wavefunctions

s: sphere, p: three dumbbells

d: more complex shapes (less stable than the p orbital in the one-outer shell)

Coffee break: 3D Periodic Table?



Do you know the 3-D periodic table ‘Elementouch’?

<http://www.ss.scphys.kyoto-u.ac.jp/elementouch/>
(sorry, only in Japanese)

Coffee break: ‘Aufbau’ principle

As electrons are added to make atoms or ions, structure follows the ‘Aufbau’ principle:

- Electrons occupy ‘orbitals’ resembling one-electron states.
- Added electrons occupy lowest energy state available.
- Must satisfy Pauli principle: two electrons cannot occupy the same state.
- Each orbital angular momentum allows $2l+1$ states, each spin allows 2 states.
- As successive electrons are added, the table is filled.
- Location of electrons is described by configuration string.

written by TK

Coffee break: Moseley’s law

For an approximated calculation of multiple-electron atoms,

$$E_{nm} = 1 \text{ Ry} \cdot (Z - \eta)^2 \left(\frac{1}{n^2} - \frac{1}{m^2} \right)$$

η : screening by inner shell e-, 0 (H-like), ~ 0.4 (He-like), and ~ 1 (neutral).
For a more precise transition list, see the database (e.g., AtomDB).

Further reading...

1. Moseley’s Modeling of X-ray Frequencies [[link](#)]

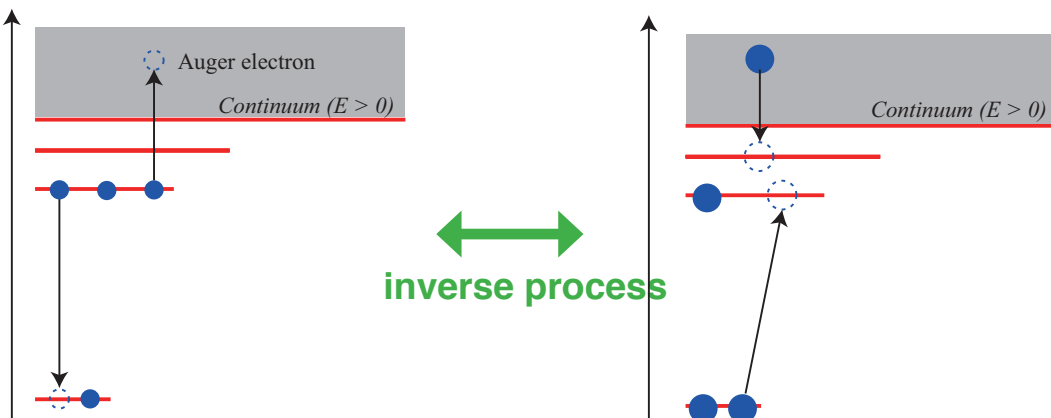
Coffee break: Importance of Precise Energies for Lines

Different physical processes become important in different energy ranges as shown in Figure 0.1 (p.3).

Example: The gravitational redshift of white dwarfs (see ASTRO-H white paper) is expected to be ~ 4 eV at the fluorescent 6.3964 keV. However, the line is a doublet 6391.0264 eV and 6404.0062 eV with an intensity ratio, 1:2. (from a slide of SM)

Inner shell atomic process

Autoionization / Dielectronic recombination



(Excitation &) Autoionization

In deexcitation, some energy is utilized from the Auger process (autoionization).

Dielectronic recombination

When a free electron is captured in a certain level of an ion, kinematic energy of the electron is utilized to make another electron bounded in the ion excited into a higher level.

Note: Innershell excitation (and subsequent autoionization) can most easily take place in alkali-metal-like states, as such ions have only one outer-shell electron.

Note: Dielectronic recombination is a resonance process, so useful for temperature diagnostics.

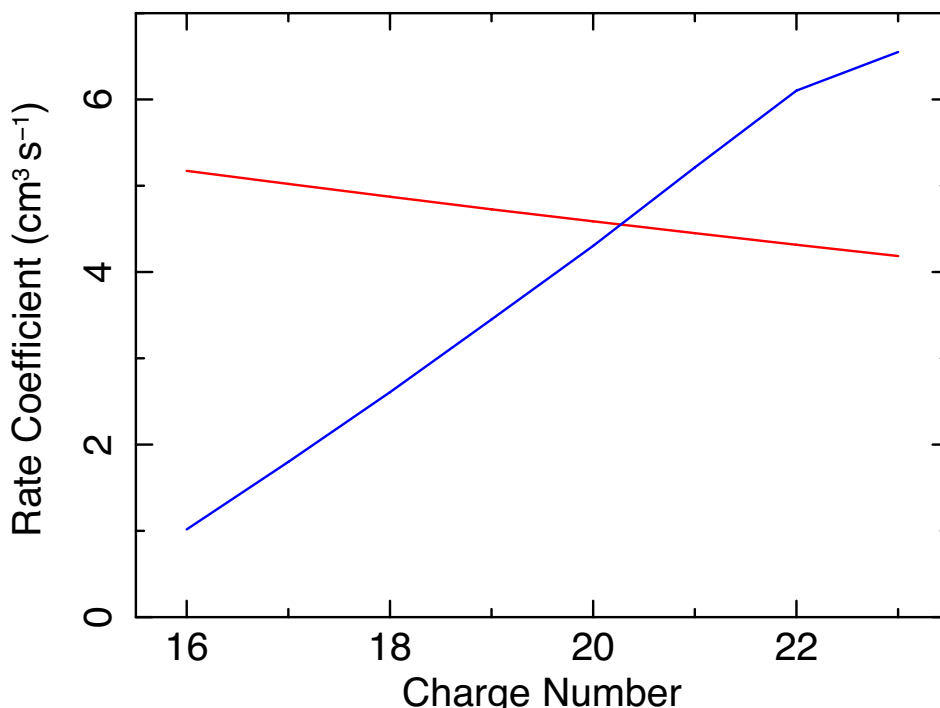


Figure: Rate coefficients of K-shell ionization (red) and total excitation (blue) for Fe ions at $kTe = 5$ keV.

Innershell ionization

■ fluorescence

Create hole in electron distribution by ionisation (through photons, electrons).

Hole filled by electron from higher shell.

Result: photon compensating energy difference.

Efficiency: fluorescence rate ω depends on nuclear charge Z .

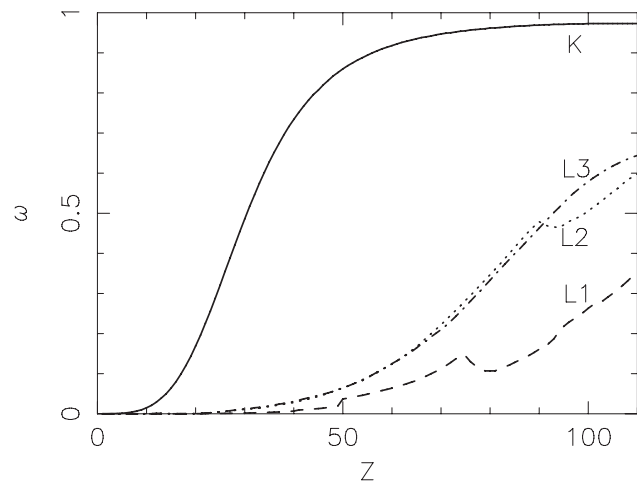
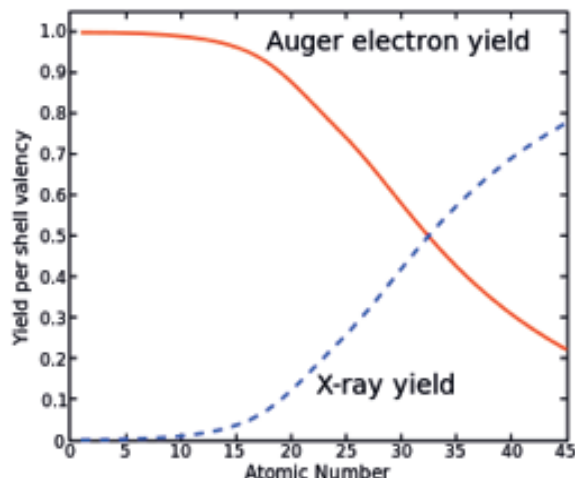


Figure: Fluorescence yield ω as a function of atomic number Z for the K and L shells.

■ Auger process



Note: Fluorescence yield is higher in the higher atomic number elements. ~0.3 for Fe, ~0.0 for O. (See NEI section for more details)

Further reading...

1. Kaastra, J. S., and Paerels, F. B. S., et al., 2008, SSRv, 134, 155 [[ADS](#)]
2. Japanese-Dutch Bilateral Workshop “Spectroscopy of Cosmic Plasma in the Era of ASTRO-H”
J. Kaastra presentation “Atomic processes” [[PDF](#)]

Topic: Nomenclature for X-ray Astrophysics

The X-ray waveband contains atomic and ionic transitions for nearly all astrophysically-abundant elements - with the notable exception of H and He. These arise primarily from transitions involving electrons in the 1s shell, but for heavier elements (*i.e.* Fe, Ni) there are transitions involving higher shells as well. This appendix contains a short discussion of spectroscopic notation combined with information on a selection of particularly strong transitions, including those from hydrogen-like and helium-like ions, Fe XVII - Fe XXIV ions, as well as fluorescent transitions from neutral atoms and ionization edges for all of the abundant elements. More information about atomic data useful for X-ray astronomy can be found at <http://www.atomdb.org>. This document is a précis of the relevant nomenclature; for fuller details, see the 1991 report by the International Union of Pure and Applied Chemistry (IUPAC) [[PDF](#)]

Spectroscopic notation

A complete discussion of spectroscopic notation is beyond the scope of this handbook; we suggest the short but highly informative text by Herzberg, "Atomic Spectra and Atomic Structure" for a more detailed review; another useful source is the "X-ray Data Booklet" published by the Center for X-ray Optics and Advanced Light Source at Lawrence Berkeley National Laboratory (website <http://xdb.lbl.gov>). X-ray astronomy is rife with poorly-used spectroscopic terminology, so following the form used by an earlier refereed paper does not guarantee proper usage.

Electron Shells: Atomic theory states that the electrons in an atom or ion are bound into "shells" with principal quantum number n starting at 1 and increasing indefinitely. The shells with quantum number $n = 1, 2, 3$, and 4 are typically referred to as the K, L, M, and N shells respectively. X-ray astronomy typically involves transitions to the K- or L-shells, although Fe M-shell transitions (*i.e.* $\Delta n = n' \rightarrow 3$) can generate photons near 0.1 keV. This nomenclature can be further divided into subshells that also give the orbital and spin angular momentum of the electrons. This is given as an integer subscript to the shell letter, but for historical reasons the value is incremented by one. Thus the L_1 shell refers to electrons with principal quantum number $n=2$ and orbital angular momentum $l=0$ (also known as '2s' shell) while the M_3 shell contains electrons with $n=3$, $l=1$, and $j=3/2$, or the $3d_{3/2}$ shell. Roman numerals (*e.g.* I, II, III) were once

used instead of Arabic for the subscript, although this usage is not deprecated.

Describing line emission

Ideally, every emission or absorption line would have a single unambiguous label that fully describes the transition. For simple systems that are well-described by LS coupling, such as helium-like ions, standard notation such as $1snl\ (^{2S+1})L_J$ can be used. This notation describes a system with one electron in the 1s shell, one in a shell with principal quantum number n and angular momentum l ; the whole system has total spin S , orbital angular momentum L , and total angular momentum J . Unfortunately, the realities of quantum mechanics, especially for complex ions with multiple electrons, makes this goal impractical. In practice, a range of different terms are used depending upon historical precedent, the bandpass at issue, and the taste or training of the author.

Before listing individual ions, it should be noted that there is a distinct difference in meaning when using Roman numerals versus Arabic superscripts. O^{6+} refers to an ion of oxygen with two bound electrons and a positive charge of 6, while O VII is a spectroscopic notation describing an emission or absorption line arising from electronic transitions within an O^{6+} ion. Thus, O VII describes a *spectrum of lines* or possibly a *photon*, while O^{6+} describes an *ion*; the two are related, obviously, but not equivalent. For example, although fully-stripped ion O^{8+} do exist, there is no such thing as a O IX photon, since no electronic transition lines can occur in an ion with no electrons. O^{8+} can, of course, radiatively recombine with an electron to form O^{7+} , but any emission lines generated thereby will be emitted by the O^{7+} ion, not O^{8+} . Finally, although the written distinction is clear, confusion can arise when speaking and so astronomers are advised to say O^{6+} as "oxygen six plus" while O VII is "Oxygen seven," especially when speaking to atomic physicists or chemists. When referring to ions, the preferred form is the number first, followed by 'plus', and not 'plus six', as described on page 11 of this report of the IUPAC [[PDF](#)].

Hydrogen-like (*i.e.* ions with a single electron) line emission follows the nomenclature used for hydrogen line emission itself. Note that the phrase "hydrogenic" should be avoided when describing these ions, since it can also mean an ion modeled using hydrogenic wave functions -- *e.g.* a Li-like ion could be approached with a hydrogenic model

if the two core $1s$ electrons were ignored. Hydrogen-like, however, will only mean a single-electron system. Transitions ending on the $n=1, 2,$ and 3 shells are described as Lyman, Balmer (or Hydrogen), and Paschen series (usually shortened to Ly, H, or Pa). Within each series, Greek letters are then used to indicate the delta of the principal quantum number for the transition, so that α, β, γ refer to $\Delta n=1, 2, 3$, respectively. Thus Ly α is the transition from $n=2 \rightarrow 1$ in a hydrogen-like ion, while Ly γ is the transition from $n=5 \rightarrow 2$ and Pa β goes from $n=5 \rightarrow 3$. These transitions are all doublets and so can be further subdivided with subscripts. These are defined so that the subscript 1 indicates the transition line with the larger total angular momentum while subscript 2 indicates the smaller angular momentum. Thus, Ly α_1 is the transition $2p\ ^2P_{3/2} \rightarrow 1s\ ^2S_{1/2}$, while Ly β_2 is the transition $3p\ ^2P_{1/2} \rightarrow 1s\ ^2S_{1/2}$.

Helium-like line emission can be described simply using standard LS notation, *i.e.* $1s3p\ ^1P_1 \rightarrow 1s^2\ ^1S_0$, although there are special cases for transitions from $n=2 \rightarrow 1$. These are listed in an upper right table. The He-like resonance lines, starting with the line ‘w’ or R, can also be described as He α , then higher series as He β , He γ , etc. The w, x, y, z notation is from [Gabriel \(1972, MNRAS, 160,99\)](#), which also includes a series of dielectronic satellite lines labelled a-v as well (see below).

Ions with more electrons become progressively more problematic because the LS-term designation breaks down due to electron-electron interactions within the ion. A common solution to this problem is to use designations developed from experimental results. For example, labels for strong lines from Fe XVII through Fe XXIV (see Table next pge) can be found in [Brown et al. \(1998, ApJ, 502, 1015\)](#), although these are not universally used.

Dielectronic recombination (DR) satellite emission lines, as mentioned above in the Helium-like case, occur when an ion has recombined non-radiatively, with the kinetic energy of the recombining electron balanced by the excitation of an existing electron. For many ions, this is the dominant form of recombination, substantially exceeding the radiative recombination rate. The recombined ion has two electrons in excited states, with a total energy exceeding the ionization energy of the system. This ion may then re-ionize, inverting the recombination process, or it can radiatively stabilize by emitting a photon. In this latter case, the atomic energy levels of the system can be described as that of the ion before recombination, albeit perturbed by the presence of the second

Table: He-like nomenclature

LSJ description	Gabriel (1972)	Common name
$1s2p\ ^1P_1 \rightarrow 1s^2\ ^1S_0$	w	R
$1s2p\ ^3P_2 \rightarrow 1s^2\ ^1S_0$	x	I ₂
$1s2p\ ^3P_1 \rightarrow 1s^2\ ^1S_0$	y	I ₁
$1s2p\ ^3S_1 \rightarrow 1s^2\ ^1S_0$	z	F

excited electron. The emitted photon will thus be similar in energy to one found in the next higher ion but will be at slightly lower energy (essentially redshifted) due to the presence of the second excited electron. As a result, such transitions are termed ‘satellites’, as they frequently occur close to a strong transition line. Thus the He-like w, x, y, and z lines have a family of satellite lines at nearly the same energies, arising from doubly-excited Li-like lines, and doubly-excited He-like ions create similar satellites around H-like Ly α lines. While generally weak, these lines can be powerful temperature and ionization state diagnostics. It should be noted, however, that while satellite lines are typically signatures of recombination, doubly-excited systems can also occur as a result of inner-shell ionization or excitation.

The notation for DR satellite lines is not well developed. In the case of Li-like systems, Gabriel (1972) described many of these transitions with the letters a-v. However, in general there is no rigorous classification system besides simply stating the energy levels of the transition.

Fluorescent emission lines can arise when an atom or ion has an inner-shell electron removed, possibly due to photoionization, electron collision, or nuclear transition. After the event, the ion is highly unstable and will rapidly fill the electron ‘hole’ with an electron from a less-bound shell, releasing energy that may ionize the ion further or emerge as a photon. The ionization case is generally termed the “Auger” process, although technically this only applies if the electron ‘hole’, the electron filling the hole, and the ionized electron all come from distinct shells, such as an L-shell electron filling a K-shell hole and ionizing an M-shell electron in the process; this is often written as a KLM transition. If the vacant hole and transitioning electron are both in the same shell (*e.g.* an LLM transition), the process is properly termed a ‘Coster-Kronig’ transition, although this nuance is often overlooked.

More usefully for the spectroscopist, the ion may radiatively stabilize with an electron transi-

Topic: Nomenclature for X-ray Astrophysics (continued)

Table: Bright Fe L-shell lines.

Ion	$\lambda(\text{\AA})$	E (keV)	Label	Transition
Fe XXIV	10.619	1.1676		$3p\ ^2P_{3/2} \rightarrow gnd$
Fe XXIII	10.981	1.1291	Be9	$2s3p\ ^1P_1 \rightarrow gnd$
Fe XXIII	11.019	1.1252	Be8	$2s3p\ ^3P_1 \rightarrow gnd$
Fe XXIV	11.029	1.1242	Li4	$3d\ ^2D_{3/2} \rightarrow 2p\ ^2P_{1/2}$
Fe XXIV	11.176	1.1094	Li3	$3d\ ^2D_{5/2} \rightarrow 2p\ ^2P_{3/2}$
Fe XVII	11.254	1.1017	5D	$2p^55d\ ^3D_1 \rightarrow gnd$
Fe XXIV	11.432	1.0845	Li1	$3s\ ^2S_{1/2} \rightarrow 2p\ ^2P_{3/2}$
Fe XXIII	11.736	1.0564	Be2	$2s3d\ ^1D_2 \rightarrow 2s2p\ ^1P_1$
Fe XXII	11.770	1.0534	B13	$2s^23d\ ^2D_{3/2} \rightarrow gnd$
Fe XVII	12.124	1.0226	4C	$2p^54d\ ^1P_1 \rightarrow gnd$
Fe XXIII	12.161	1.0195	Be1	$2s3s\ ^1S_0 \rightarrow 2s2p\ ^1P_1$
Fe XVII	12.266	1.0108	4D	$2p^54d\ ^3D_1 \rightarrow gnd$
Fe XXI	12.284	1.0093	C10	$2s^22p3d\ ^3D_1 \rightarrow gnd$
Fe XXI	12.393	1.0004	C8	$2s^22p3d\ ^3D_1 \rightarrow 2s^22p^2\ ^3P_1$
Fe XXII	12.754	0.9721	B4	$2s2p_{1/2}3s \rightarrow 2s2p^2\ ^2D_{3/2}$
Fe XX	12.846	0.9652	N31	$2s^22p_{1/2}2p_{3/2}3d_{3/2} \rightarrow gnd$
Fe XX	12.864	0.9638	N31	$2s^22p_{1/2}2p_{3/2}3d_{5/2} \rightarrow gnd$
Fe XXI	12.822	0.9670	C4	$2s2p_{1/2}2p_{3/2}3d_{5/2} \rightarrow 2s2p^3\ ^3D_1$
Fe XX	12.824	0.9668	N31	$2s^22p_{1/2}2p_{3/2}3d_{3/2} \rightarrow gnd$
Fe XX	12.912	0.9602	N30	$2s^22p_{1/2}2p_{3/2}3d_{5/2} \rightarrow gnd$
Fe XX	12.965	0.9563	N29	$2s^22p_{1/2}2p_{3/2}3d_{3/2} \rightarrow gnd$
Fe XX	13.061	0.9493	N26	$2s^22p_{1/2}^23d_{5/2} \rightarrow gnd$
Fe XIX	13.462	0.9210	O26	$2s^22p^3(^2D)3d\ ^3S_1 \rightarrow gnd$
Fe XIX	13.497	0.9186	O25	$2s^22p^3(^2D)3d\ ^3P_2 \rightarrow gnd$
Fe XXI	13.507	0.9179	C3	$2s2p_{1/2}^23s \rightarrow 2s2p^3\ ^3D_1$
Fe XIX	13.518	0.9172	O24	$2s^22p^3(^2D)3d\ ^3D_3 \rightarrow gnd$
Fe XIX	13.795	0.8988	O19	$2s^22p^3(^4S)3d\ ^3D_3 \rightarrow gnd$
Fe XVII	13.825	0.8968	3A	$2s2p^63p\ ^1P_1 \rightarrow gnd$
Fe XXI	14.008	0.8851	C1	$2s^22p_{1/2}3p_{1/2} \rightarrow 2s2p^3\ ^3D_1$
Fe XVIII	14.208	0.8726	F20	$2s^22p^4(^1D)3d\ ^2D_{5/2} \rightarrow gnd$
Fe XVIII	14.208	0.8726	F20	$2s^22p^4(^1D)3d\ ^2D_{3/2} \rightarrow gnd$
Fe XVIII	14.256	0.8697	F19	$2s^22p^4(^1D)3d\ ^2S_{1/2} \rightarrow gnd$
Fe XX	14.267	0.8690	N9	$2s2p_{1/2}^22p_{3/2}3s \rightarrow 2s2p^4\ ^4P_{5/2}$
Fe XVIII	14.373	0.8626	F17	$2s^22p^4(^3P)3d\ ^2D_{5/2} \rightarrow gnd$
Fe XVIII	14.534	0.8531	F15	$2s^22p^4(^3P)3d\ ^2F_{5/2} \rightarrow gnd$
Fe XIX	14.664	0.8455	O13	$2s^22p^3(^2D)3s\ ^3D_3 \rightarrow gnd$
Fe XVII	15.014	0.8258	3C	$2p^53d\ ^1P_1 \rightarrow gnd$
Fe XIX	15.079	0.8222	O8	$2s^22p^3(^4S)3s\ ^5S_2 \rightarrow gnd$
Fe XIX	15.198	0.8158	O5	$2s2p_{1/2}^22p_{3/2}^23s \rightarrow 2s2p^5\ ^3P_2$
Fe XVII	15.261	0.8124	3D	$2p^53d\ ^3D_1 \rightarrow gnd$
Fe XVII	15.453	0.8023	3E	$2p^53d\ ^3P_1 \rightarrow gnd$
Fe XVIII	15.625	0.7935	F11	$2s^22p^4(^1D)3s\ ^2D_{5/2} \rightarrow gnd$
Fe XVIII	15.824	0.7835	F9	$2s^22p^4(^3P)3s\ ^4P_{3/2} \rightarrow gnd$
Fe XVIII	16.004	0.7747	F6	$2s^22p^4(^3P)3s\ ^2P_{3/2} \rightarrow gnd$
Fe XVIII	16.071	0.7715	F4	$2s^22p^4(^3P)3s\ ^4P_{5/2} \rightarrow gnd$
Fe XIX	16.110	0.7696	O2	$2s^22p_{1/2}2p_{3/2}^23p_{1/2} \rightarrow 2s2p^5\ ^3P_2$
Fe XVIII	16.159	0.7673	F3	$2s2p^53s\ ^2P_{3/2} \rightarrow 2s2p^6\ ^2S_{1/2}$
Fe XVII	16.780	0.7389	3F	$2p^53s\ ^1P_1 \rightarrow gnd$
Fe XVII	17.051	0.7271	3G	$2p^53s\ ^3P_1 \rightarrow gnd$
Fe XVII	17.096	0.7252	M2	$2p^53s\ ^3P_2 \rightarrow gnd$
Fe XVIII	17.623	0.7035	F1	$2s^22p^43p\ ^2P_{3/2} \rightarrow 2s2p^6\ ^2S_{1/2}$

tion that emits a ‘fluorescent’ photon. The relative probability of ionization vs fluorescence depends primarily upon the nuclear charge; low-Z elements overwhelmingly tend to ionize, while iron with a K-shell hole has a ~30% chance of emitting a photon and elements much heavier than iron strongly tend towards fluorescence. Fluorescence lines are described first by the shell of the electron hole, so an ‘Fe K’ line refers to a transition ending with an electron moving to the K-shell. Much like hydrogen-like ions, this can be refined with a Greek letter such as α or β to indicate the Δn of the tran-

sition, so that a $K\alpha$ transition arises from a $n=2 \rightarrow 1$ transition and $K\beta$ from $n=3 \rightarrow 1$. A subscript to the Greek letter further subdivides the transitions; see the 1991 IUPAC report for details. This Greek-letter nomenclature is from Siegbahn and is still in common use. The IUPAC has developed an alternative nomenclature which can also be used although it is less common; see Table VIII.2 of [PDF] for details.

(written by RS, GB, TE, AF, JK, and TK)
[contribution is also listed at the last page]

Further reading...

1. Gabriel, A., H., 1972, *MNRAS*, 160, 99 [[ADS](#)]
2. Brown, G. V., et al. 1998, *ApJ*, 502, 1015 [[ADS](#)]
3. IUPAC (International Union of Pure and Applied Chemistry, R. Jenkins et al.), “Part VIII. Nomenclature system for X-ray spectroscopy, Recommendations 1991”, 1991 [[PDF](#)]
4. IUPAC “Nomenclature of Inorganic Chemistry” 1970 [[PDF](#)]

Coffee break: The names of the 1s-np transitions

The 1s-np transitions are named as follows:

Iso-electronic sequence	Transition	Proper name	Wrong name
H	1s-2p	Ly α	K α
H	1s-3p	Ly β	K β
He	1s-2p (resonance)	w (He α)	K α
He	1s-2p (intercombination)	x, y	K α
He	1s-2p (forbidden)	z	
He	1s-3p (res)	He β	K β
Li and higher	1s-2p	K α	
Li and higher	1s-3p	K β	

Further reading,

1. Japanese-Dutch Bilateral Workshop “Spectroscopy of Cosmic Plasma in the Era of ASTRO-H”
J. Kaastra presentation “Atomic processes” [[PDF](#)]

Astrophysical Plasma

Topic: Various astrophysical plasmas have a wide range of electron density and temperature. They are classified into collisional or photo-ionized plasmas which show different spectral signatures. Several plasma codes and fitting packages are provided to quantitatively investigate the plasma conditions.

Various astrophysical plasma

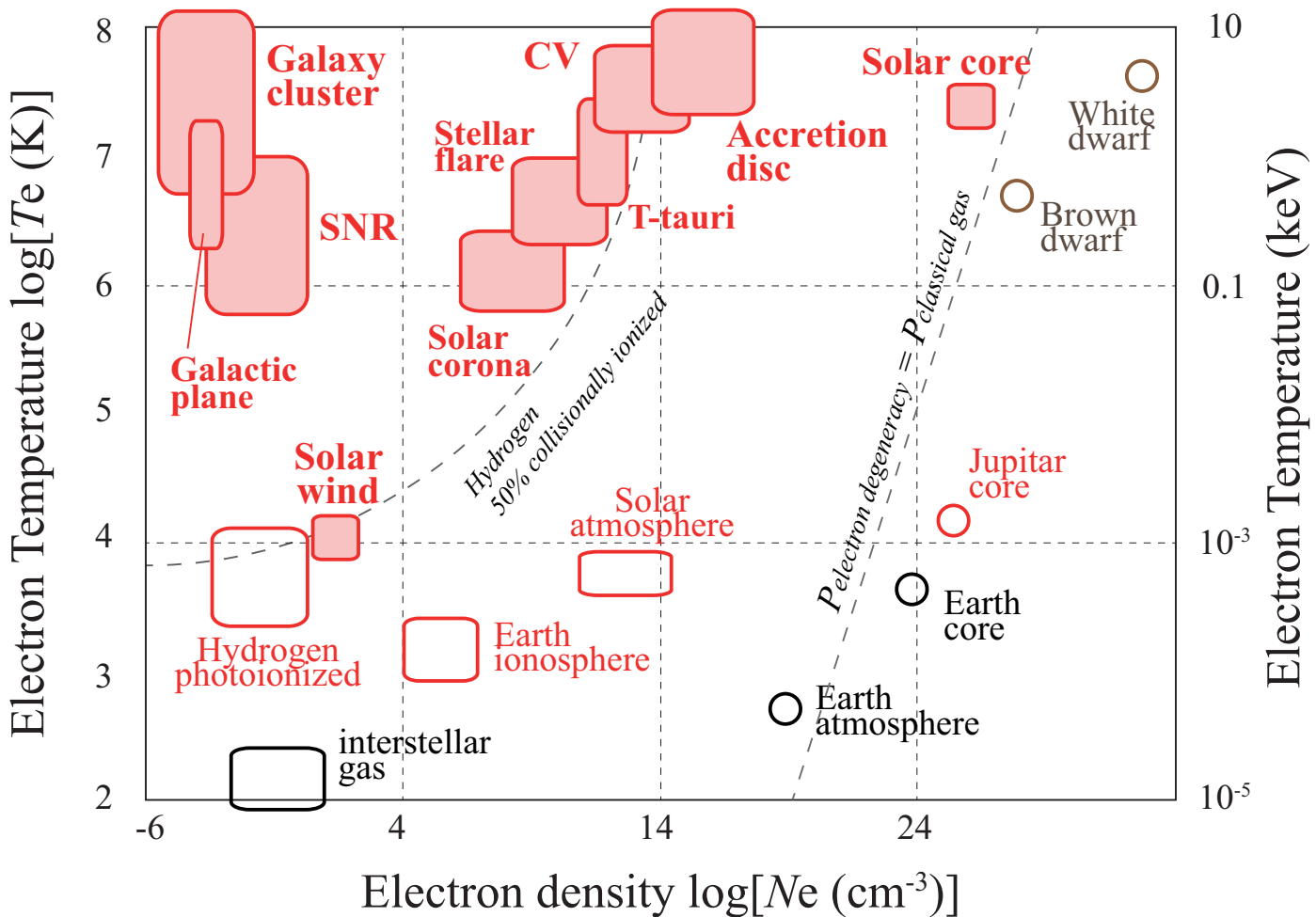


Figure 4.1: Various astrophysical plasma on different free electron temperature T_e and density N_e regimes. Red filled regions are highly-ionized plasma, open red regions are weakly-ionized plasma or highly-dense plasma. Black symbols represent neutral material for comparison (modified from Pradhan & Nahar, 2011).

Atomic processes determines ionization balance. For example, the collisional case is

$$\frac{dn_i}{dt} = n_e \cdot (q_{i-1}n_{i-1} - (q_i + a_i)n_i + a_{i+1}n_{i+1})$$

where q_i and a_i are ionization and recombination rate coefficient. Set of coupled linear equations gives the ion charge state of a given element. $dn_i/dt=0$ is an equilibrium.

Collisional plasma		Photo-ionized plasma
$kTe \sim I_E$ (ionization)		$kTe \ll I_E$ (ionization)
Coronal (Nebular)	Collisional-radiative	Radiative-driven
$N_e < 10^{14-16} \text{ cm}^{-3}$	$10^{14-15} < N_e < 10^{27} \text{ cm}^{-3}$	
Collisions excite ions but are too rare to de-excite them. Decays are purely radiative. This is also called the “ground-state” approximation, where all ions are assumed to be in the ground-state when collisions occur.	Collisions compete with photons in de-exciting levels. A level with a small A value may be collisionally de-excited before it can radiate.	Since photons ionizes plasma, no need of $kTe \sim I_E$. Photo-ionized plasma is typically cool ($kTe \sim 0.1 I_E$). Radiative recombination continua (RRC) is a simple and robust spectroscopic signature of recombining plasma.

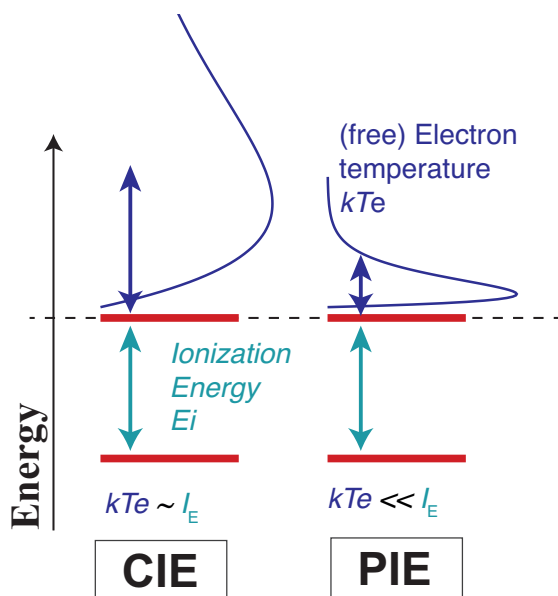


Figure 4.2: Schematic view of energy levels under **collisional ionization equilibrium (CIE)** and **photo-ionized equilibrium (PIE)**.

The **CIE** is a balance between collisional ionization (CI) and radiative recombination (RR) + dielectric recombination (DR). Examples are galaxy clusters, supernova remnant, and stellar coronae.

The **PIE** is a balance between photoionization (PI) and RR+DR. Examples are broad line region of AGN, planetary nebulae of white dwarfs, and stellar wind around X-ray binaries.

Coffee break: Plasma Codes and Spectral Fitting Packages

1. Plasma codes developed from collisional ionized plasma
 - Mekal [[link](#)] (MEwe et al. 1985 [[ADS](#)], KAstra et al. 1992, Liedahl., 1995 [[ADS](#)])
 - CHIANTI [[link](#)] (Landini & Monsignori Fossi 1970 [[ADS](#)], Firenze et al., 2006)
 - AtomDB [[link](#)] (APEC [[link](#)]; Raymond & Smith 1977 [[ADS](#)], Smith et al. 2001 + APED [[ADS](#)])
2. Plasma codes developed from photoionized plasma
 - XSTAR [[link](#)] (Kallman et al., 1982 [[ADS](#)], Kallman & Bautist 2001 [[ADS](#)])
 - Cloudy [[link](#)] (Ferland et al., 1998 [[ADS](#)], 2013 [[ADS](#)])
 - MOCASSIN (Ercolano et al., 2008 [[ADS](#)])
3. Spectral fitting packages
 - Xspec [[link](#)]
 - SPEX [[link](#)] (Kaastra et al., 1996 [[ADS](#)])
 - Sherpa (Part of CIAO; [link](#))
 - ISIS (MIT Chandra HETG group for grating data; [link](#))

Collisional Ionization Equilibrium (CIE)

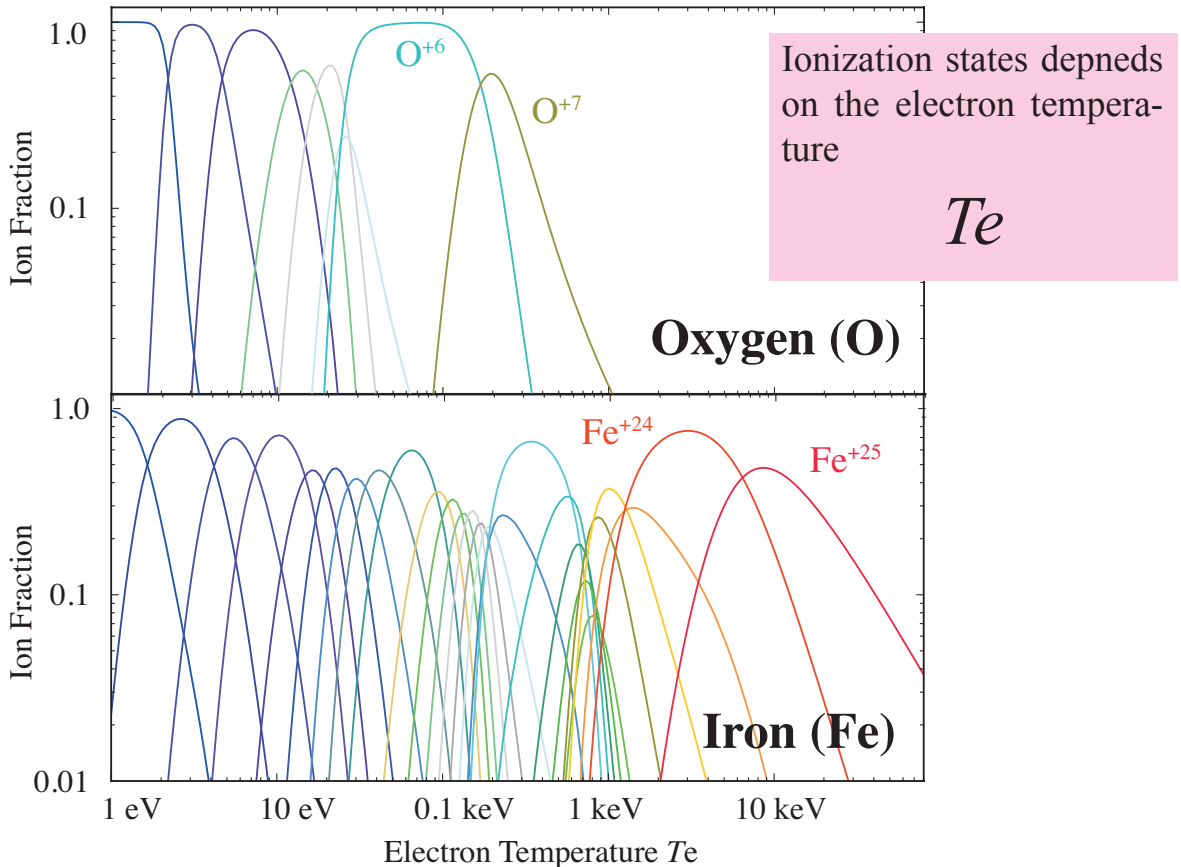


Figure 4.3: Ion fractions for gas in collisional ionization equilibrium, for the elements oxygen and iron. Ion fractions from neutral to hydrogen-like are shown as functions of the electron kinetic temperature kT_e . Sample curves are labeled; others can be derived using the fact that adjacent ion stages arise in sequence as temperature is increased or decreased. These curves were calculated using the rates reported in Bryans et al. 2009 ApJ 691 1540.

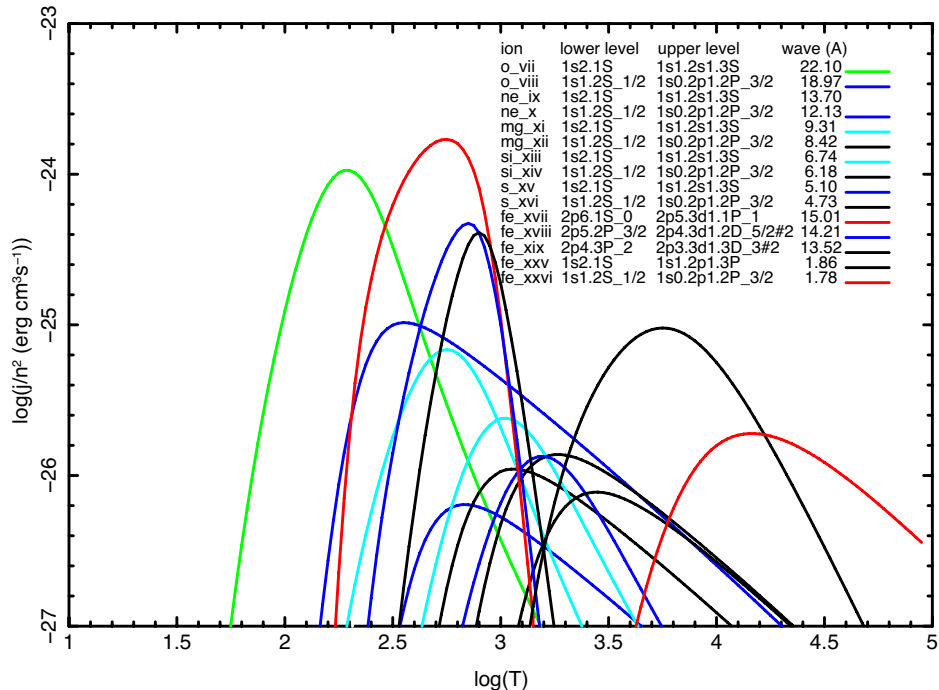


Figure 4.4: Emissivities for selected strong lines of abundant heavy elements for gas in collisional ionization equilibrium. Vertical axis is the log of the emissivity divided by density squared. Horizontal axis is log of gas temperature in units of 10^4 K. Curves were calculated using the ion fractions in figure 1 together with the excitation rate coefficients from Chianti (Landi et al., 2013 ApJ 763 86).

Photo Ionization Equilibrium (PIE)

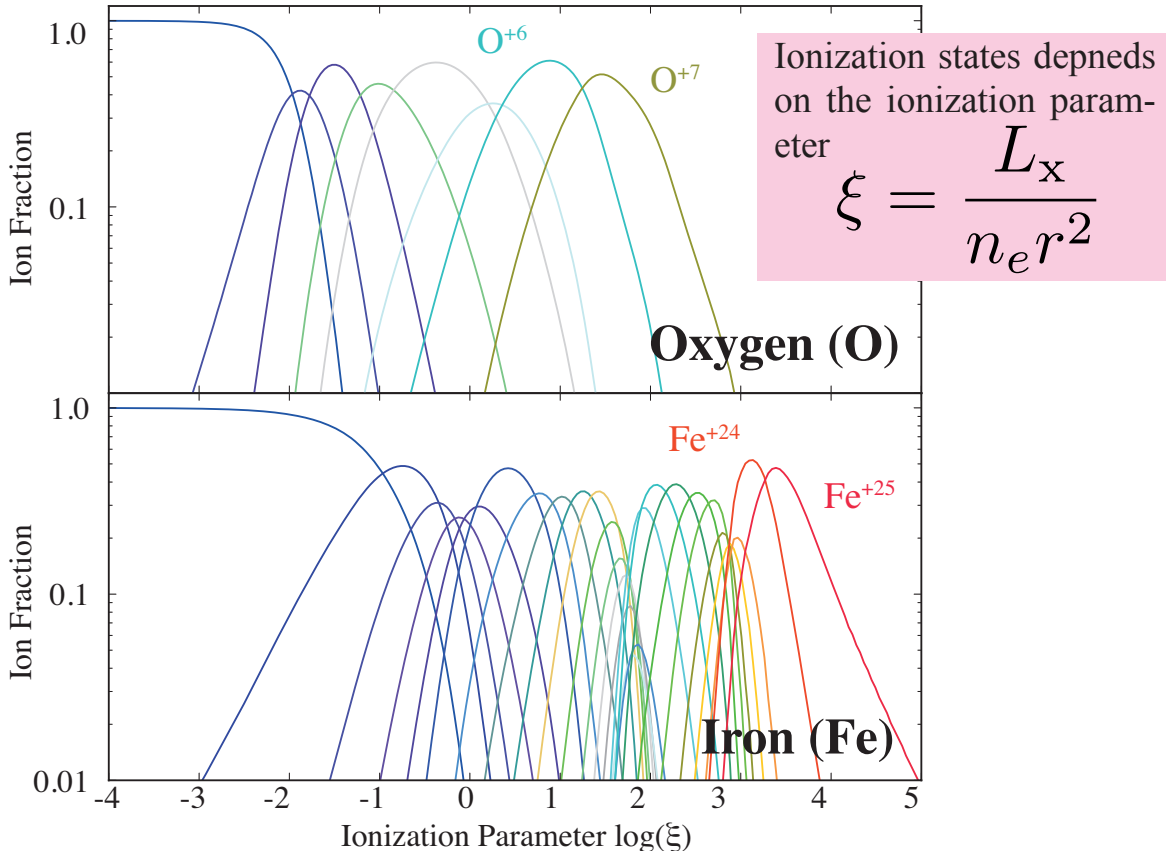


Figure 4.5: Ion fractions for gas in coIon fractions for gas in photoionization equilibrium, for the elements oxygen and iron. Ion fractions from neutral to hydrogen-like are shown as functions of ionization parameter $\xi = 4\pi F/n$. Sample curves are labeled; others can be derived using the fact that adjacent ion stages arise in sequence as ionization parameter is increased or decreased. These curves were calculated using the rates reported in Kallman and Bautista 2001 ApJS 133 221 and Kallman et al., 2004 ApJS 155 675.

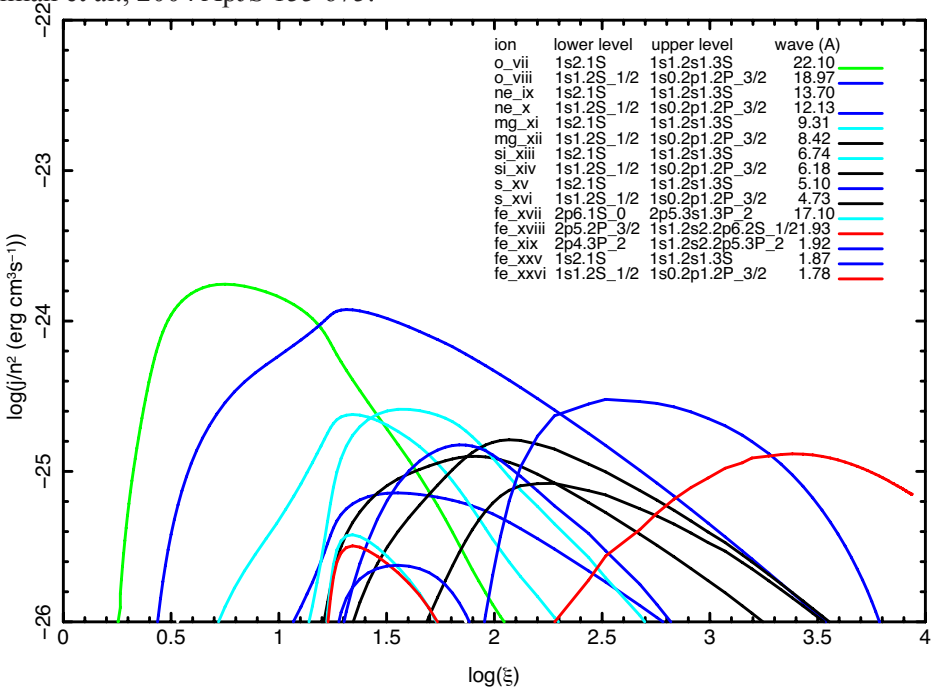
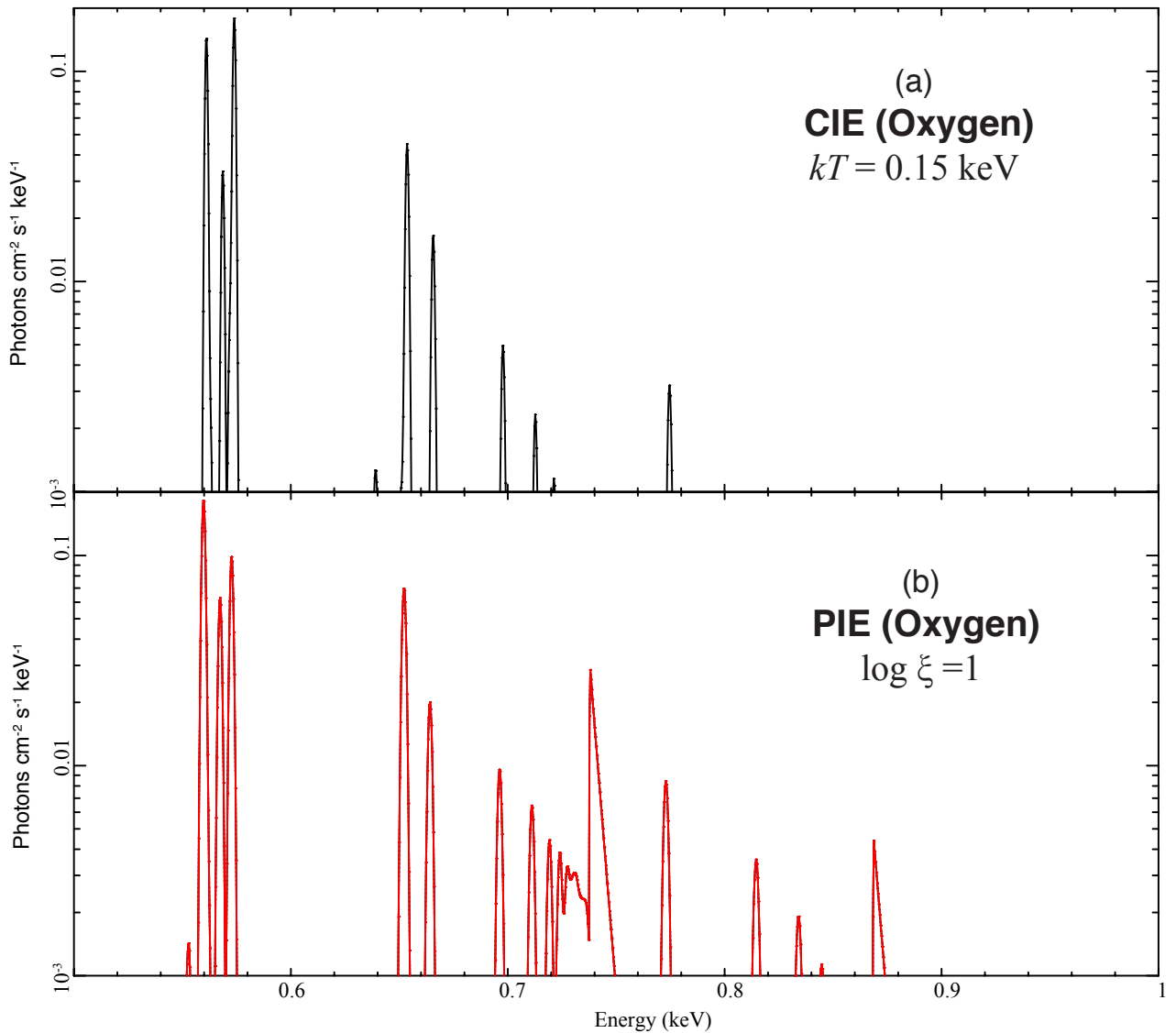


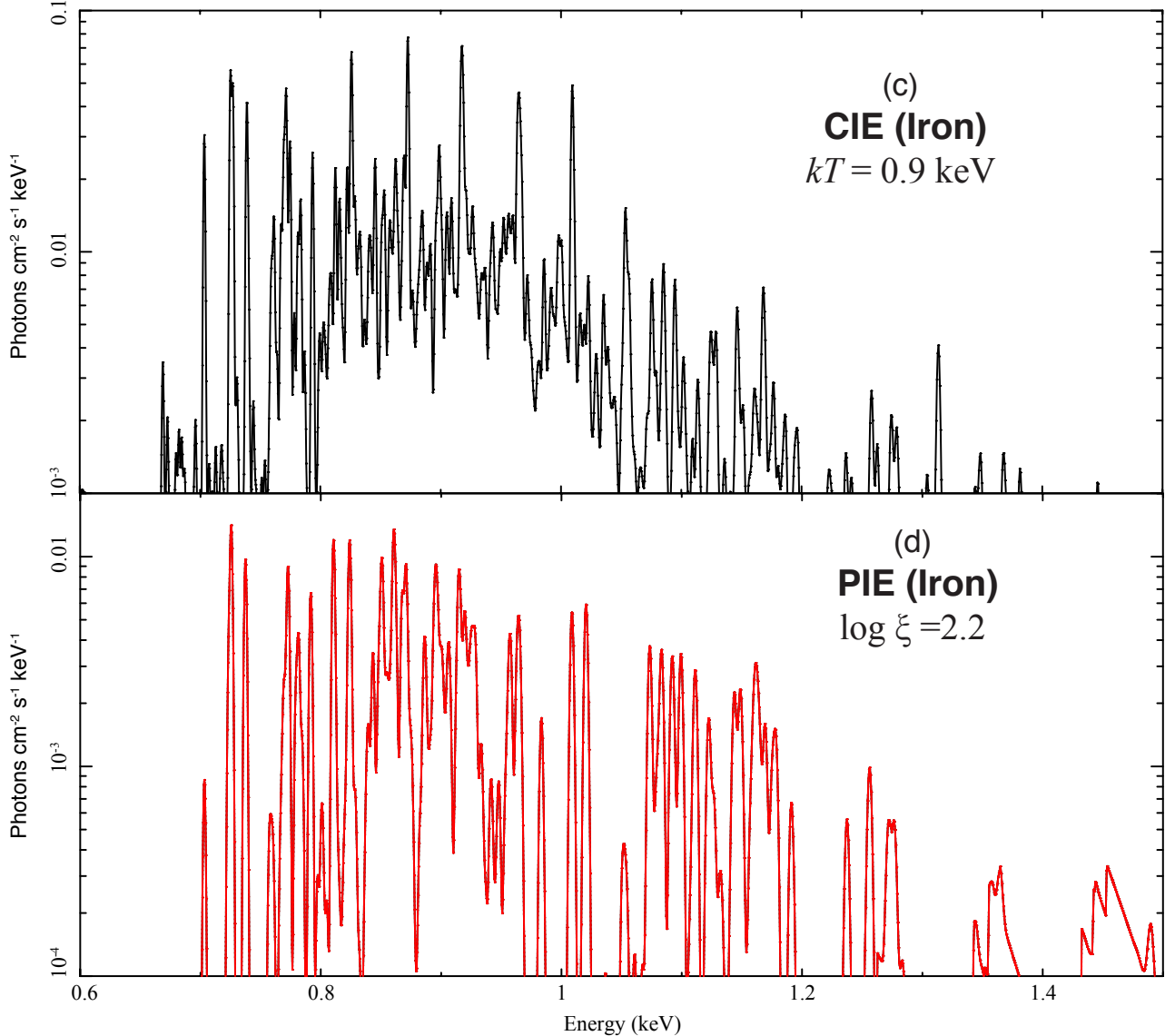
Figure 4.6: Emissivities for selected strong lines of abundant heavy elements for gas in photoionization equilibrium. Vertical axis is the log of the emissivity divided by density squared. Horizontal axis is log of ionization parameter $\xi = 4\pi F/n$. Curves were calculated using the ion fractions in figure 3 together with the excitation rate coefficients reported in Kallman and Bautista 2001 ApJS 133 221 and Kallman et al., 2004 ApJS 155 675.

Spectral Examples of CIE and PIE



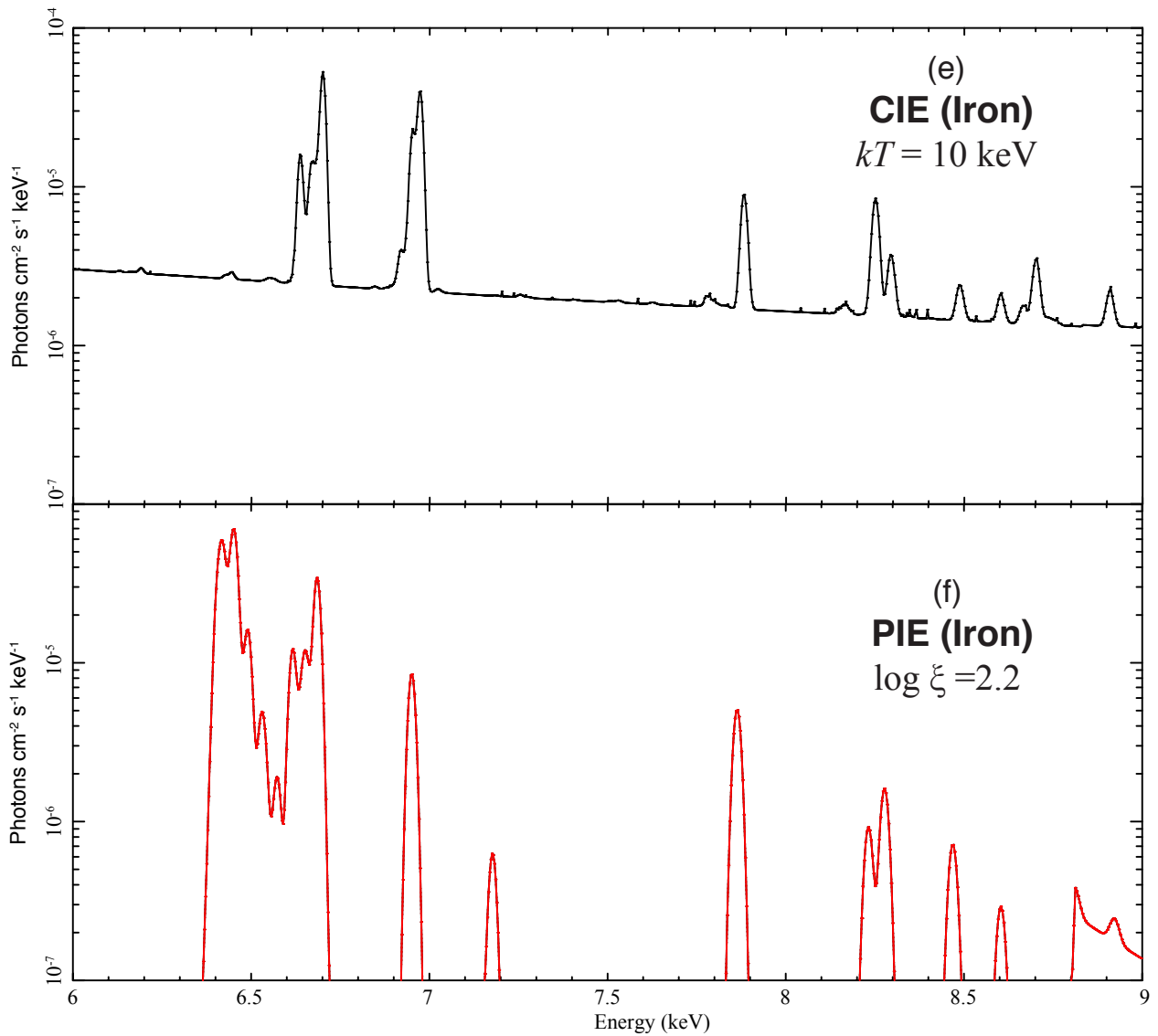
Top: Emission spectrum from a collisional plasma at temperature $kT=0.15$ keV. Emission is from only O ions; This temperature is chosen to produce lines from O^{7+} and O^{6+} (H-like and He-like) which are roughly comparable. This figure can be compared with the panel b (PIE, right). Turbulent line broadening of 300 km s^{-1} is assumed. Prominent lines include O^{6+} triplet lines near 0.56 keV; note that the resonance line is stronger than the forbidden or intercombination. Also note the O^{7+} L α line near 0.65 keV. Comparison with the panel b (PIE, right) shows that the collisional plasma has a much steeper decrement in the Rydberg series of both ions, and the RRCs are too weak to show on this plot.

Bottom: Emission spectrum from a photoionized plasma at $\log \xi = 1$, density 10^4 cm^{-3} . Emission is from only O ions; at this ionization parameter the lines from O^{7+} and O^{6+} (H-like and He-like) are roughly comparable. Turbulent line broadening of 300 km s^{-1} is assumed. Prominent lines include O^{6+} triplet lines near 0.56 keV; note that the forbidden line is stronger than the resonance or intercombination. Also note the O^{7+} L α line near 0.65 keV, the O^{6+} Rydberg series leading to the O^{6+} RRC near 0.74 keV, and the O^{7+} Rydberg series leading to the RRC near 0.85 keV.



Top: Emission spectrum from a collisional plasma at temperature $kT=0.9 \text{ keV}$. Emission is from only Fe ions; at this ionization parameter the lines from Fe^{16+} are prominent. Turbulent line broadening of 300 km s^{-1} is assumed. Prominent lines include Fe^{16+} near 0.73 keV and 0.83 keV . Note that the 0.83 keV is stronger. Regularly spaced strong lines from adjacent ions are apparent.

Bottom: Emission spectrum from a photoionized plasma at $\log \xi = 2.2$, density 10^4 cm^{-3} . Emission is from only Fe ions; at this ionization parameter the lines from Fe^{16+} are prominent. Turbulent line broadening of 300 km s^{-1} is assumed. Prominent lines include Fe^{16+} near 0.73 keV and 0.83 keV . Note that the 0.73 keV is stronger due to recombination cascade. RRCs near 1.35 and 1.45 keV are apparent. Other ions also show evidence of recombination, which tends to distribute emission among



Top: Emission spectrum from a collisional plasma at temperature $kT=10$ keV is shown in the energy range 6 - 9 keV. Emission is from only Fe ions. Turbulent line broadening of 300 km s^{-1} is assumed. H-like and He-like Fe are apparent, but lower ion stages are absent; collisional plasmas generally do not make strong K line emission from Fe ion stages lower than He-like. The strong bremsstrahlung continuum produced by this gas is also apparent.

Bottom: Emission spectrum from a photoionized plasma at $\log \xi = 2.2$, density 10^4 cm^{-3} is shown in the energy range 6 - 9 keV. Emission is from only Fe ions; at this ionization parameter the lines from ions ranging from Fe^{16+} to hydrogenic are prominent. Turbulent line broadening of 300 km s^{-1} is assumed. Lines from Fe^{16+} to Fe^{23+} blend together between 6.4 keV and 6.6 keV. Emission from He-like and H-like Fe is apparent at 6.7 and 6.97 keV. Higher Rydberg lines and RRCs are apparent above 7 keV.

written by TK

Non-Equilibrium Ionization (NEI)

Definition: ionization rate $\text{noneq. recombination rate}$

Ionization age: $n_e t \text{ (cm}^{-3}\text{s)}$

n_e : electron density in plasma t : elapsed time since the gas was shock-headed

Plasma achieves CIE at $n_e t \gtrsim 3 \times 10^{12} \text{ cm}^{-3}\text{s}$

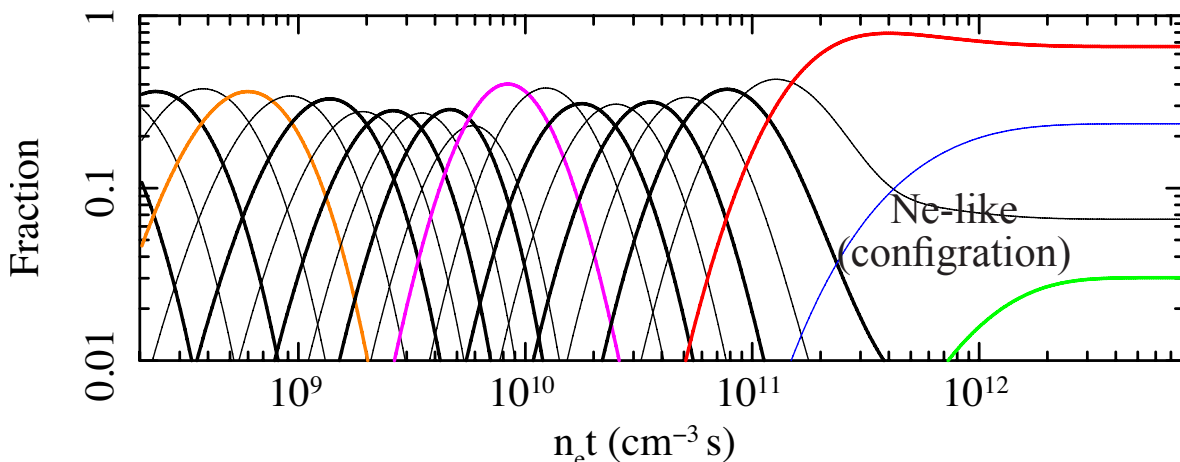


Figure: Ion fraction of Fe in an NEI plasma with $kTe = 5 \text{ keV}$

In a CIE plasma at 5 keV, most Fe atoms are in the He-like state, and little Fe are in ionization states below Li-like. This is because the average kinetic energy of free electrons in the 5 keV plasma is much higher than the L-shell ionization potential (~1 keV) and comparable to K-shell ionization potential (~7-10 keV).

In an NEI plasma, on the other hand, while the free electrons are energetic enough to ionize the K-shell bound electrons, there are a number of low-ionized atoms that still have outer shell electrons. Therefore, innershell processes (innershell ionization and fluorescence) are important, particularly for Fe-peak elements (relatively high fluorescence yields). This is the characteristic of the NEI plasma in the point of view of spectroscopy. The fluorescence emission offers useful diagnostics for NEI plasma.

Example: Fe K β /K α emissivity ratio

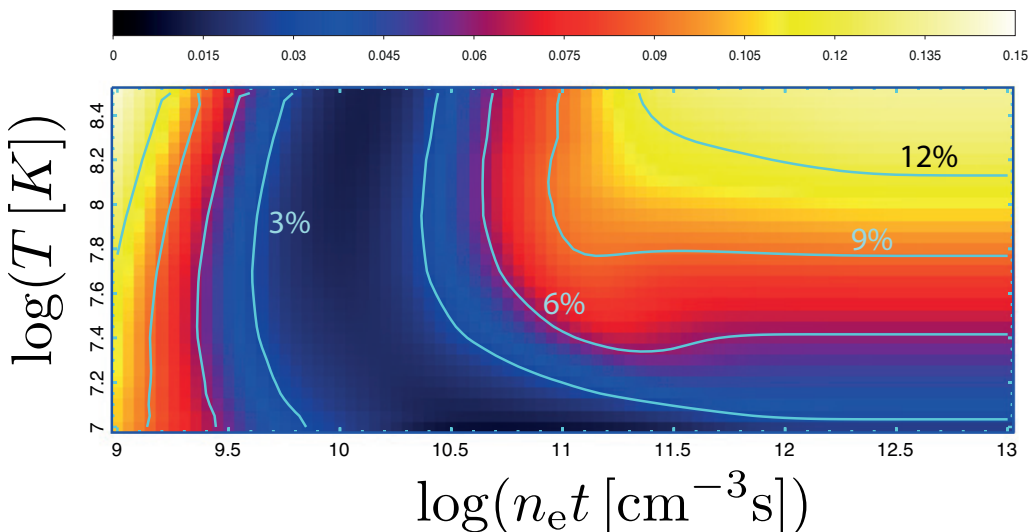


Figure: Fe K β /K α emissivity ratio

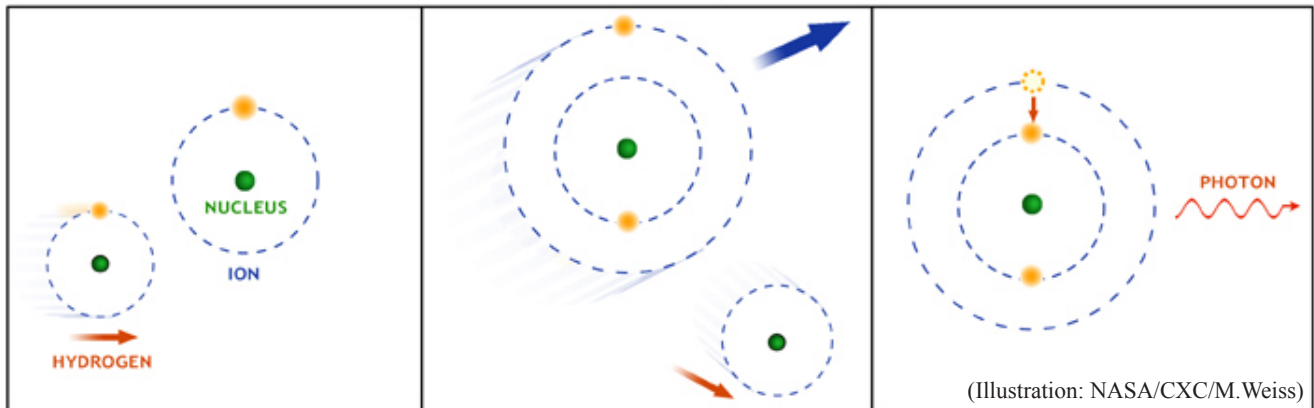
In the low-ionization regime ($\log(n_e t) < 10$):

- ratio drops with ionization, because Fe loses 3p shell electrons
- ratio doesn't depend on temperature, because ionization is dominant

In the high-ionization regime ($\log(n_e t) > 10$):

- ratio goes up with ionization, because Fe loses 2p shell electrons
- ratio strongly depends on temperature, because excitation is dominant

Topic: Charge Exchange



0. We know a lot about CX, but the predicted spectra are still uncertain!
1. Total cross section $\sigma \sim q \times 10^{-15} \text{ cm}^2$
2. The n-selective cross section σ_n is strongly peaked for $n \sim q^{3/4}$
(See Fig A; from figure 3.2 of Janev & Winter)
3. For high collision energies $\gtrsim 1 \text{ keV/amu}$, l distribution is statistical
4. For lower collision energies ($\sim 100 \text{ eV/amu}$), l distribution peaks at low l .
Classically, the low collision velocity limits the angular momentum accessible for typical impact parameters.
(points 3 and 4 are illustrated in Fig B., figure 12 of Wargelin et al.)
5. The resulting spectrum depends on cascades from the capturing levels:
6. See Examples

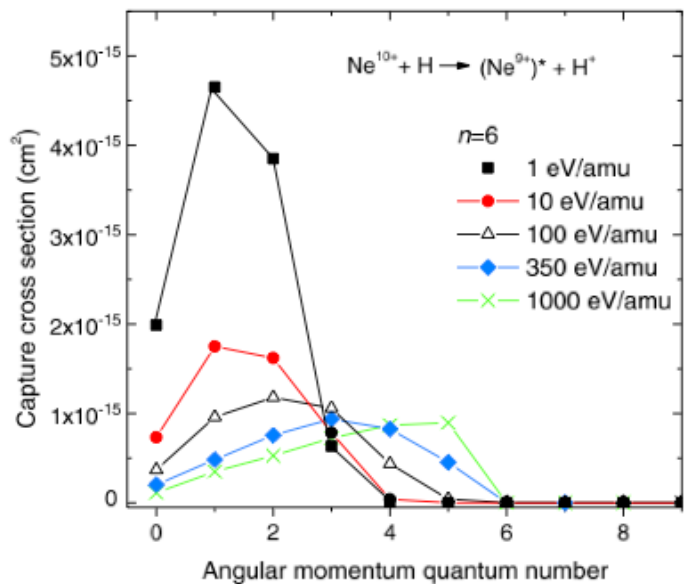
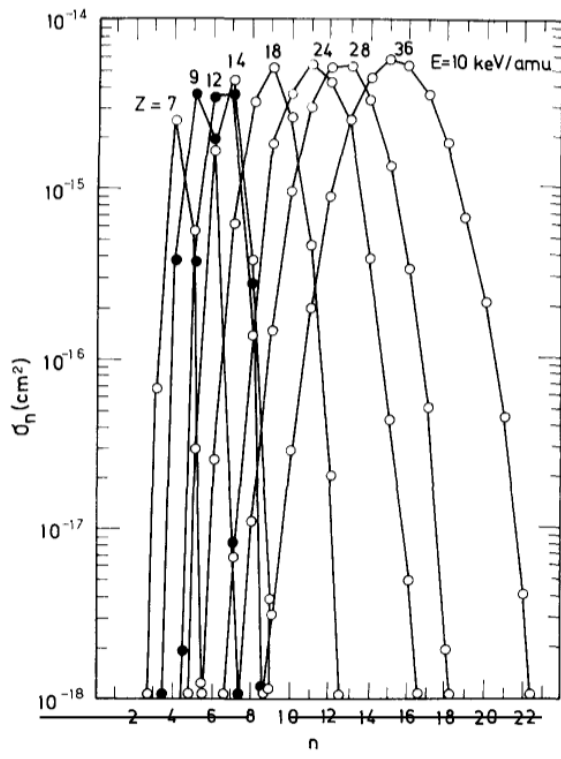


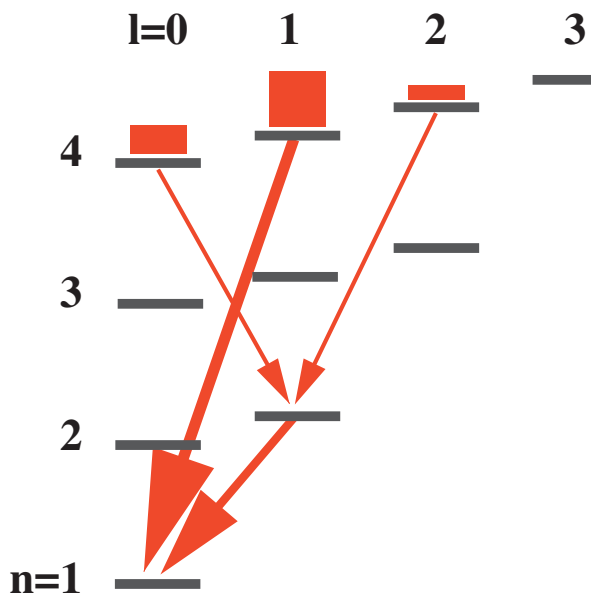
Fig. A

Fig. B

[1] R.K. Janev & H. Winter, Physics Reports (1985) [\[ADS\]](#)

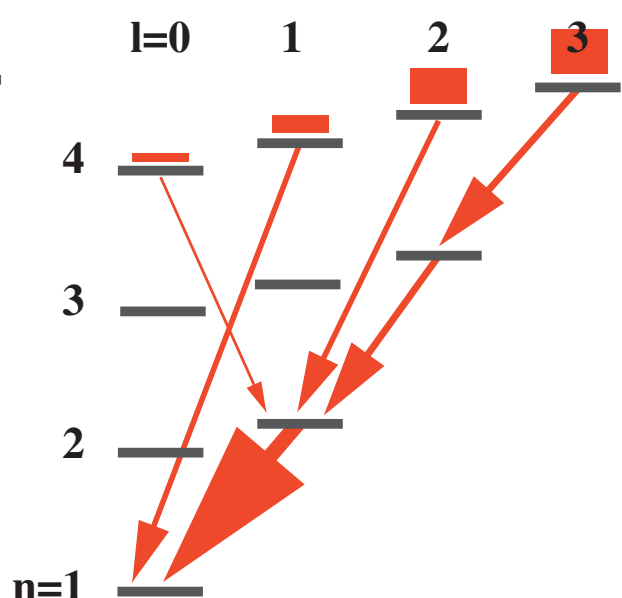
[2] B.J. Wargelin, P. Beiersdorfer, and G. V. Brown, CaJPh (2008) [\[ADS\]](#)

atomic H + bare ion \rightarrow X-ray line from H-like ion



low collision velocity

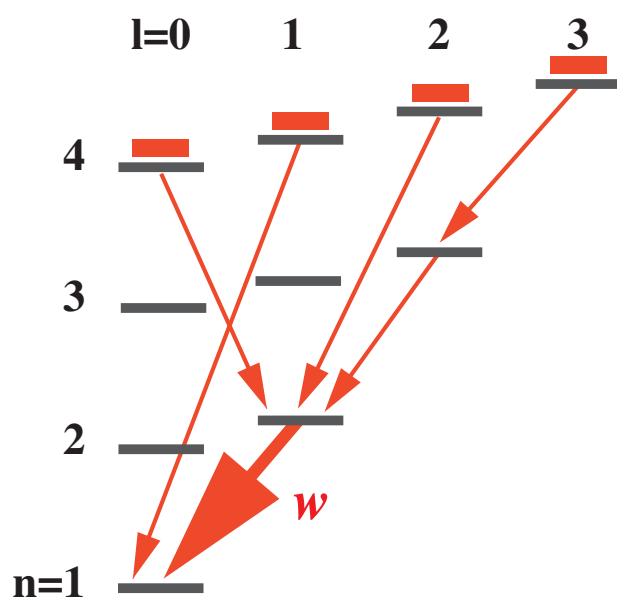
capture into $l=1$ is strong;
capture into $n_{\max}=4$ is strong;
 \Rightarrow Lyman gamma ($4p \rightarrow 1s$) is strong



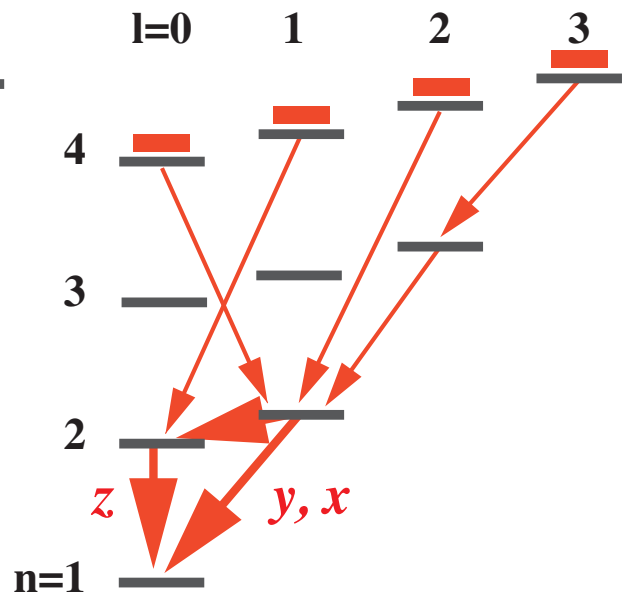
high collision velocity

capture into $l=1$ is weak;
capture into $n_{\max}=4$ is strong;
 \Rightarrow Lyman alpha is strong

atomic H + H-like ion \rightarrow X-ray line from He-like ion



any collision velocity
singlet (~25% of captures)
 $\Rightarrow w$ is strong; some n_{\max} p $\Rightarrow 1s$



any collision velocity
triplet (~75% of captures)
 $\Rightarrow xyz$ are strong; ratio depends on l distribution

Conclusion: for He-like $G=(x+y+z)/w \sim 3$

Absorption

Topic: High resolution X-ray spectra provide rich information of absorption or scattering by interstellar medium (ISM). These pages are prepared for our future editing of this cookbook.

Absorption

X-ray spectra can be produced by a variety of processes, including radiative decay of ions which are excited by collisions with thermal electrons, and also recombination of ions with electrons which are created by photoionization. X-ray photons can also interact with the gas which produced them, or other gas. This occurs via photoionization, in which a photon is absorbed while ionizing an ion from the ground state, or by resonant excitation in which a photon excites an electron between two bound levels. The importance of absorption is described by the optical depth, which is the integral of the product of the gas density and the absorption cross section along the line of sight: $\tau = \int n\sigma dz$.

The importance of absorption can be established observationally: the cross section for absorption by neutral interstellar material is approximately $\sigma_{ISM} = 1.5 \times 10^{-21} E_{keV}^{-3} cm^{-2}$ (Morrison and McCammon 1980; Wilms et al., 2000) where E_{keV} is the photon energy in keV. The effects of this preferential absorption of lower energies is apparent in essentially every X-ray spectrum.

Absorption in bound-bound transitions is observed from many compact objects, i.e. AGN and X-ray binaries. The energies of the absorption features are consistent with partially ionized material, and a Doppler blue-shift indicating outflow. These are denoted as warm absorbers (e.g. Kaspi et al., 2002). This also introduces the important distinction between true absorption, in which the photon is destroyed, and scattering. In elastic scattering the photon is re-emitted following absorption, with essentially the same energy, but with a different direction.

It is important to note that any detection of net absorption implies either a non-spherical distribution of gas around the source of radiation which is being absorbed, or else a net outflow or inflow of that gas, or else true absorption or inelastic scattering. That is, if a point source of radiation is surrounded by a stationary spherically symmetric cloud of gas which only scatters elastically, then the cloud has no net effect on the radiation seen by an outside observer. Every photon which is removed from the primary beam of radiation from the center to the observer is balanced by a photon which is scattered into that beam somewhere else in the spherical cloud. Since elastic scattering occurs in many strong lines in warm absorbers, their detection implies that the absorber is not spherically symmetric around the central source of radiation. (by TC)

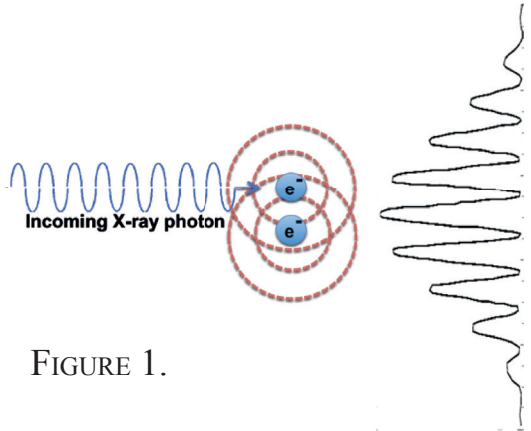


FIGURE 1.

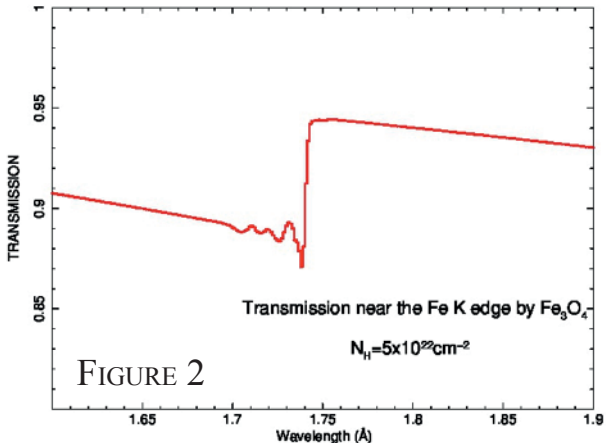
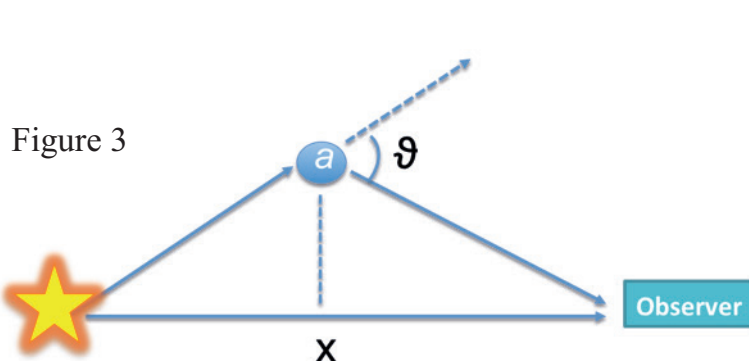


FIGURE 2

Figure 1: Photoelectric absorption works differently if the medium absorbing the X-rays is constituted not only by gas but also by dust grains. This is the case in the interstellar medium (ISM), where elements with atomic number higher than 6 (e.g. C, O, Fe, Mg and Si) are partially or totally in dust form. The X-ray light from Galactic objects is influenced by absorption from the intervening medium.

In the figure, the interaction between the incoming X-ray photon and the electron inside the dust grain are depicted. The X-ray photons kick off the innermost electron. This is the well-known photoelectric effect. But since the dust grain is dense, the electron will be influenced by all the electrons of the neighboring atoms. In quantum physics, electrons can be described by a wave function. This wave will have positive and negative interference with the other electron-waves, creating a diffraction pattern. The shape of such diffraction pattern is a function of the number of electrons surrounding the atom and their distance from the nucleus. In high-resolution X-ray spectra, extra narrow features, called XAFS (X-ray Absorption Fine Structure), produced by the interference pattern of the electrons, are visible within the photoelectric edge shape (Ueda et al. 2004, Lee et al. 2005, 2009, Pinto et al. 2010, Costantini et al. 2012). This is shown in **Figure 2**, where the transmission of incoming X-rays absorbed by dust is shown around the Fe K edge ($E=7.1$ keV). Here a high column density and an iron depletion (i.e. $\text{Fe}_{\text{dust}}/(\text{Fe}_{\text{dust}} + \text{Fe}_{\text{gas}})$) of 90% are assumed.



$$I_{\text{sca}}(\theta) = F_x N_H \int_{E_{\min}}^{E_{\max}} dE S(E) \int_{a_{\min}}^{a_{\max}} da n(a) \int_0^{1-\theta} \frac{f(x)}{(1-x)^2} \left(\frac{d\sigma(E, a, \theta)}{d\Omega} \right) dx$$

Figure 3: X-ray radiation is not only absorbed by the intervening interstellar dust, but also scattered. Extinction of light is therefore simply the sum of these two processes. In the figure, the geometry of the scattering is displayed. The X-ray photon meet the dust grain and is scattered at an angle θ . The scattering from the multitude of grains of different size and located at different distances along our line of sight, will produce a halo of scattered radiation around the source.

The radial distribution and intensity of the scattered radiation will depend on several parameters, as shown in the equation. F_x and N_H are the source flux and the total column density along the line of sight. The intensity will be also dependent on the spectral shape of the source, the dust size distribution and the geometrical distribution of the dust along the line of sight. The parameter $d\sigma/d\Omega$ is the differential scattering cross section, which is a function of the energy of the X-ray photon, the size and finally the fractional distance of the grain (Predehl & Schmitt 1995, Smith & Dwek 1998, Costantini et al. 2005). Every Galactic source will be influenced, with varying degree, by the scattering along the line of sight. (by EC)

References:

- Costantini, E., Freyberg, M.J. & Predehl, P. 2005, A&A, 444, 187
Costantini, E. et al. 2012, A&A, 539, 32
Lee, J. et al. 2009, ApJ, 702, 970

Lee, J. & Ravel, B. 2005, ApJ, 622, 970

Pinto, C. et al. 2010, A&A, 521, 79

Predehl, P. & Schmitt, J.H.M.M. 1995, A&A, 293, 889

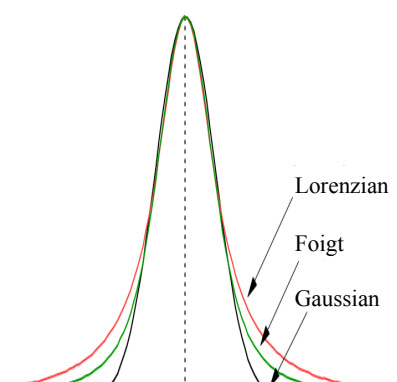
Smith, R.K. & Dwek, E., ApJ, 1998, 503, 831

Ueda, Y. et al. 2005, ApJ, 620, 274

Line Widths and Shifts

Topic: In the first part, essential three functions, which can explain line widths resulted by thermal motions, responses, and life times of excitation states, are introduced. In the second part, line shifts by cosmic expansion, bulk motions of matters, and effects of strong gravity, are summarized.

Line profile and width

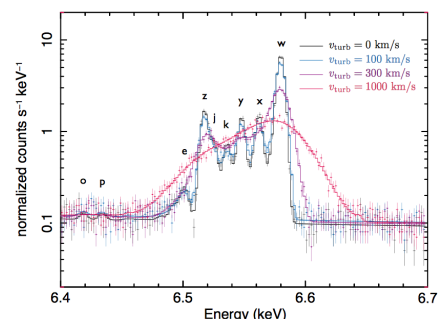
Gaussian function	Lorenzian function	Foigt function
$G(E) = \exp\left(-\frac{m}{2k_B T} \left(\frac{E - E_0}{E_0}\right)^2 c^2\right)$	$L(E) = \frac{h^2 \gamma / 8\pi^3}{(E - E_0)^2 + (h\gamma / 4\pi)^2}$	$V(E) = \int_{-\infty}^{+\infty} G(E') L(E - E') dE'$
Line broadening due to detector responses follows the gaussian distribution. Atoms in thermal motions give the Maxwellian distribution. Then, the doppler broadening, of all atoms follows gaussian distribution. E : Energy in rest frame E_0 : Observed energy m : Electron mass T : Temperature c : Light velocity k_B : Boltzmann constant	Emission line production follows the uncertainty principle of $\Delta E \Delta t > h/2\pi$. The natural line profile is obtained as a Lorenzian distribution by Fourier transform against the possibility function in which $1/\Delta t$ is a life time of an excitation state. E : Energy in rest frame E_0 : Observed energy h : Plank constant γ : $1/\Delta t$ where Δt is life time	Convolution of Gaussian and Lorenzian. Actual line profile. 
Thermal broadening width		Natural width
$\Delta E = \frac{2E_0}{ch} \left(\frac{2k_B T \ln 2}{m} \right)^{1/2}$		$\Delta E = \frac{h}{2\pi\Delta t(Z)} = \frac{h}{2\pi\tau} = hA(Z)$

This figure from <https://www.wavemetrics.com/products/igorpro/dataanalysis/peak-analysis/multippeakfitting.htm>

Coffee break: Turbulence expected in cluster of galaxies

When gas includes turbulent parts, a line profile is changed as following the equation below. Especially in cluster of galaxies, the turbulent velocity is expected to be measured by this broadening.

$$\Delta E = \sqrt{8 \ln 2} \left(\frac{v_{\text{turb}}}{c} \right) E = 5.3 \text{ eV} \left(\frac{v_{\text{turb}}}{100 \text{ km/s}} \right) \left(\frac{E}{6.7 \text{ keV}} \right)$$

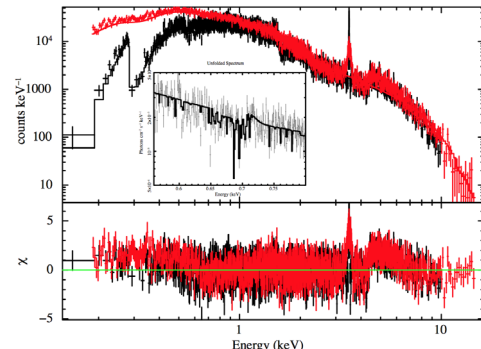


Line energy shift

Cosmic redshift	Doppler shift	Gravitational redshift
$E = E_0(1 + z)$	$E = E_0 \frac{1 - (V \cos \theta)/c}{\sqrt{1 - V^2/c^2}}$	$E = \frac{E_0}{1 - GM/c^2 R}$
A center energy shift between observed energy E_0 to energy in rest frame E , due to the cosmic expansion. Further objects are more strongly affected.	A center energy shift between observed energy E_0 to energy in rest frame E , by a bulk motion of matters or objects with velocity V . Its degree changes with the eye direction θ and the ratio between V and the light velocity c .	A center energy shifts between observed energy E_0 to energy in rest frame E , due to time delays of the general relativity effect near a massive object with a mass of M . With the gravitational constant G and the light velocity c , the shift at a radius R can be derived.

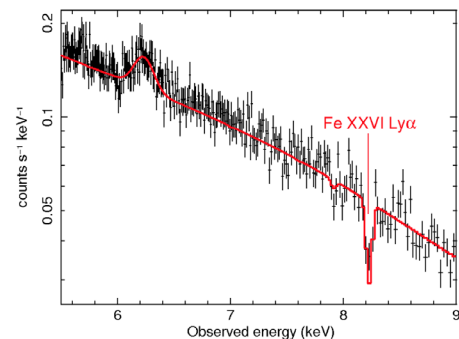
Coffee break: Cosmic redshift seen in GRB afterglow

Gamma-bursts (GRBs) may have afterglows with X-ray spectra shown in right figure, which was simultaneous with the SXS (black) and SXI (red) assuming the 100 ksec exposure. If Fe-K α emission line and edge features are observed, they are expected to be significantly shifted to lower energies due to cosmic redshift. We can estimate the redshifts of GRBs by utilizing the energy shift.



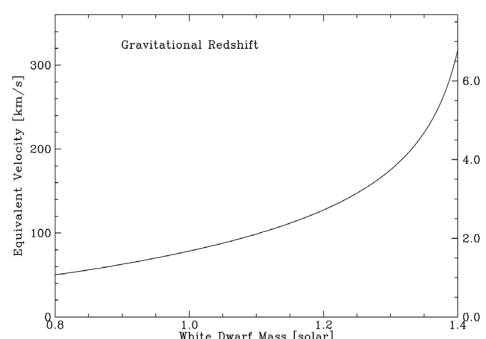
Coffee break: Doppler shift by outflows in AGNs

In active galactic nuclei, we sometimes observe spectral lines from matters moving from a center to outer regions, called Ultra-Fast Outflows (UFOs) with velocities of several tens percent of the light speed c . Right figure shows an SXS 100 ks simulation of a H-like Fe absorption line by an UFO in Mrk 509. It shifted from 6.97 to \sim 8.2 keV due to a bulk motion of an UFO with the velocity of \sim 0.2 c . With the SXS, we can identify physical properties including velocities, ionization degrees, and column densities of the UFOs.



Coffee break: WD mass estimation by gravitational redshift

Cataclysmic variables emit hard X-rays from hot plasmas formed by mass accretions onto surfaces of white dwarfs (WDs). The hard X-ray irradiates the WD surface and an accretion disk, and a neutral Fe-K α emission line is produced. If a WD has a relatively high mass close to the Chandrasekhar mass limit, the Fe-K α emission line is expected to shift its center energy due to the gravitational redshift. When the WD mass is 1.4 times solar mass, the energy shift is predicted to become \sim 6.5 eV, as shown in right figure.



Topic: Spectral signature hints and flowchart



Figure: Interpretation of a given spectrum which is a priori unknown can be summarized in the form of a flowchart or expert diagram. The measurable quantities associated with a line feature can be used to distinguish between various scenarios for the physical conditions in the gas producing the feature. These include coronal equilibrium, photoionized, coronal non-equilibrium, and cold gas. The choice between these scenarios can be summarized, crudely, in terms of a set of questions or measurable quantities associated with the line feature. These can be described in the form of a flowchart. This is illustrated in the diagram; the final boxes in red describe the model which could be used to fit the spectrum within xspec, spex or an equivalent analysis environment. It should be emphasized that such a diagram is designed to be primarily illustrative; it cannot possibly capture the many different line features that can arise in a given spectrum.

Topic: ASTRO-H White Paper Science

ASTRO-H white papers and subdivided themes introduced in 9th science meeting

0. Introduction [ADS]

1. Stars -Accretion, Shocks, Charge Exchanges and Magnetic Phenomena [ADS]

Dynamics on/around Stars [[pdf](#)], Colling Winds in Massive Stars [[pdf](#)], Diffuse Emission from the Massive Star Forming Regions [[pdf](#)]

2. White dwarfs [ADS]

Magnetic CVs studied with Fe XXV triplet lines [[pdf](#)], Gravitational Redshift of the 6.4 keV Line as a Proof of near Chandrasekhar Mass White Dwarf [[pdf](#)], Origin of Dwarf Novae in Outburst [[pdf](#)]

3. Low-mass binaries [ADS]

Mass/Radius of Neutron Stars [[link](#)],

Winds from Accreting Neutron Stars Origin of Broad Iron Line? [[pdf](#)]

4. Accreting Pulsars, Magnetars, and Related Sources [ADS] poster I [[pdf](#)], II [[pdf](#)], III [[pdf](#)]

5-6. Stellar-Mass Black Holes [ADS]

Black hole spin [[pdf](#)], Accretion disk wind [[pdf](#)], Low-frequency variability [[pdf](#)],
Accretion flow evolution [[link](#)], Super-Eddington accretion [[pdf](#)]

7. Young Supernova Remnants [ADS]

Typing SNRs and Unveiling their Progenitors [[pdf](#)], Ejecta Distribution in Space and Velocity & Shock Physics [[pdf](#)], Young SNRs are efficient cosmic ray accelerators [[pdf](#)]

8. Older Supernova Remnants and Pulsar Wind Nebulae [ADS]

Physics of ISM-dominated Limb-Brightened SNRs [[pdf](#)],

Pulsar Wind Nebulae and their evolution [[pdf](#)], Mixed Morphology SNRs [[ppt](#)]

9. Plasma Diagnostic and Dynamics of the Galactic Center Region [ADS]

Relic of the Sagittarius A* Activity [[pdf](#)], X-ray Study on the Activity History of Sagittarius A* by Three-dimensional View of the Galactic Center [[pdf](#)], Hard X-ray Diagnosis of the Galactic Center Complex [[pdf](#)]

10. High Resolution Spectroscopy of Interstellar and Circumgalactic Gas in the Milky Way and Other Galaxies [ADS]

High Resolution Spectroscopy of Interstellar and Circumgalactic Gas in the Milky Way and Other Galaxies [[pdf](#)]

11-14. Clusters of Galaxies and Related Science [ADS]

The Perseus Cluster [[pdf](#)], AGN Feedback in the Virgo Cluster [[pdf](#)], Chemical Composition & Evolution of Galaxy Clusters [[pdf](#)], Mapping Gas Flows and Turbulence in Merging Galaxy Clusters [[pdf](#)], Galaxy Clusters:Measuring Non-thermal Pressure and Mass [[pdf](#)], Detecting and characterizing the Warm-Hot Intergalactic Medium (WHIM) [[pdf](#)], X-ray Hunt for Dark Matter [[pdf](#)], Sterile neutrino dark matter [[pdf](#)]

15. AGN Reflection [ADS]

Compton Thin AGNs [[pdf](#)], Nature of Compton Thick AGNs [[pdf](#)], Probe of Strong Gravity [[pdf](#)]

16. AGN Winds [ADS]

AGN outflows [[pdf](#)], Observations of Ultra-Fast Outflow [[pdf](#)]

17. New Spectral Features [ADS]

The Physics of Charge Exchange & Charge Exchange in the Solar System and Beyond [[pdf](#)], Photoionized Plasma & Radiative Transfer [[pdf](#)], Advanced Spectral Modeling: Collisional Plasmas [[pdf](#)], Nuclear Gamma-ray Lines and Solar Neutrons [[pdf](#)]

18. Shock and Acceleration [ADS]

Shock Acceleration in SNR [[pdf](#)], Extreme Particle Acceleration in Compact Binaries [[pdf](#)]

19. Broad-band Spectroscopy and Polarimetry [ADS] poster I [[pdf](#)], II [[pdf](#)], III [[pdf](#)]

20. Chemical Evolution in High-z Universe [ADS] poster I [[pdf](#)], II [[pdf](#)]

Topic: Spectral Garely

- Browsing Interface for RGS Data [link] (XMM-Newton)
 - Bensch, K., et al. "High Resolution X-ray Spectra; A Diagnostic Tool of the Hot Universe" [ADS][slide]

Welcome to BiRD
Browsing Interface for RGS Data

Updated with all public data taken until 24th April 2014

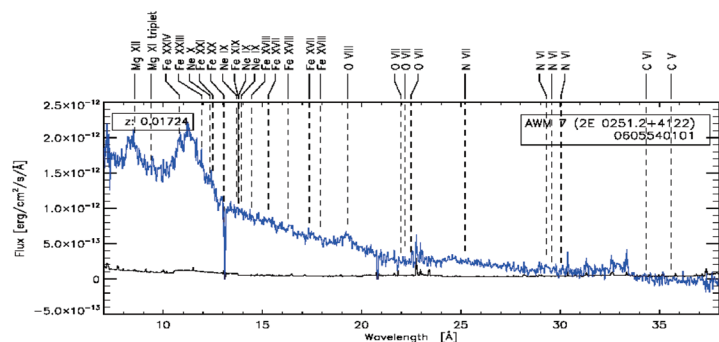
BiRD is a browsing and visualization tool for XMM-Newton RGS fluxed spectra. It allows the user to browse and examine the data before downloading them from the XSA for full analysis (more...)

Query Form

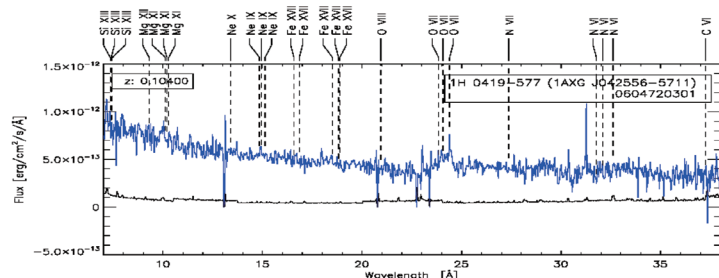
XSA	OM SUSS	2XMMi	XMMSL1
TGCat	X-Atlas		

Last update: 19th May 2014 R. González-Riestra and P.M. Rodríguez-Pascual

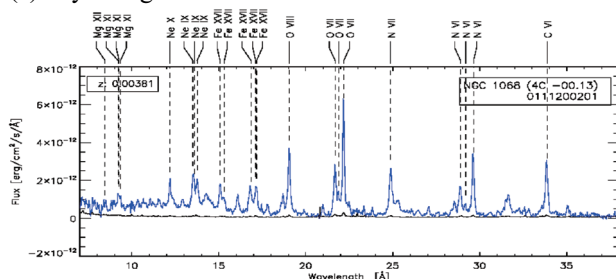
(a) Cluster of galaxies



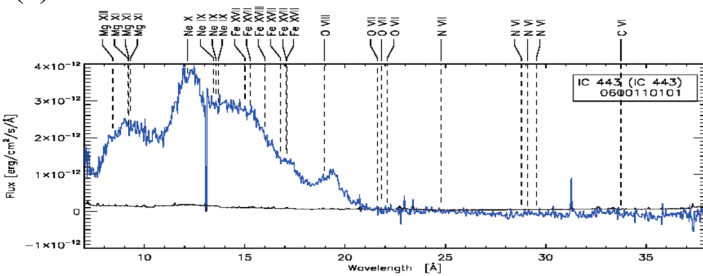
(b) Seyfert 1 galaxies



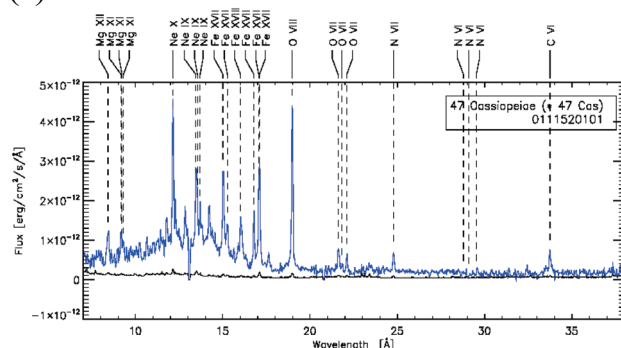
(c) Seyfert 2 galaxies



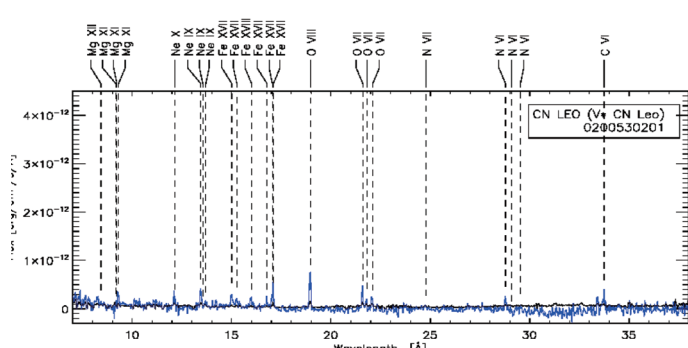
(d) SNR



(e) Emission lines stars

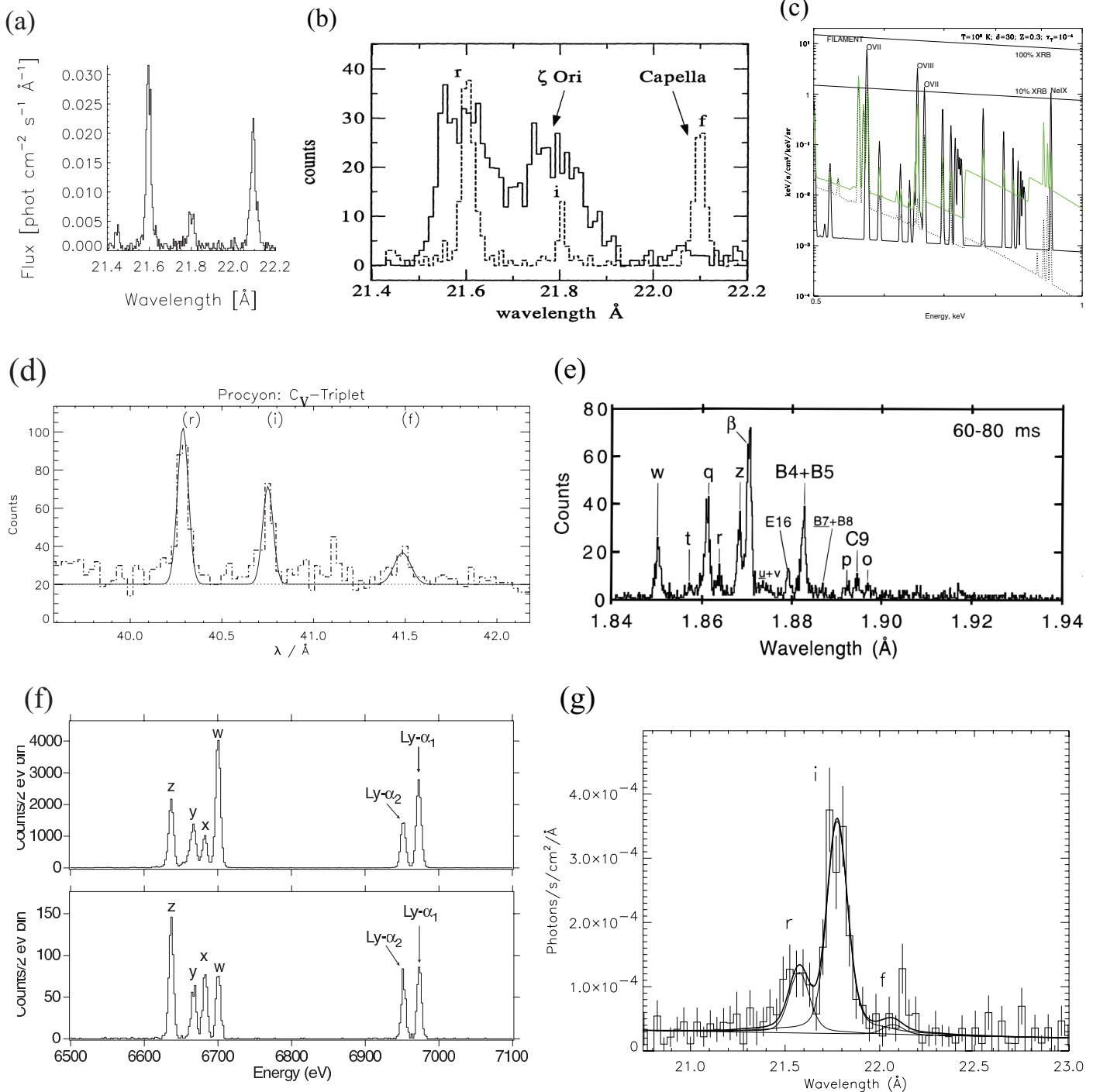


(e) Flare stars



■ Spectral garalley of He-triplet

Quiz: A Gallarey of He-like Triplets



Reference of these figures

- (a) Capella: Canizares et al., ApJL, 539, L41 (2000) [[ADS](#)]
- (b) ζ Ori: Waldron & Cassinelli, ASP Conf. Proc., 262, 69 (2002) [[ADS](#)]
- (c) IGM: Churazov et al., SSRv, 157, 193, (2010) [[ADS](#)]
- (d) Procyon: J.-U. Ness et al., A&A, 367, 282 (2001) [[ADS](#)]
- (e) EBIT: Decaux et al., ApJ, 482, 1076 (1997) [[ADS](#)]
- (f) EBIT: Wargelin et al., Can. J.Phys., 86, 151 (2008) [[ADS](#)]
- (g) EXO0748-676: Cottam et al., A&A, 365, L277 (2001) [[ADS](#)]

Example: Iron Lines from an X-ray Binary Centaurus X-3

Question: How does the accretion flow affect the evolution of a neutron star and the binary system?

Centaurus X-3 (Cen X-3) is a well known bright High Mass X-ray Binary (HMXB) with 2.1 day orbital period, composed of a 4.8-second X-ray pulsar and an O-type supergiant companion.

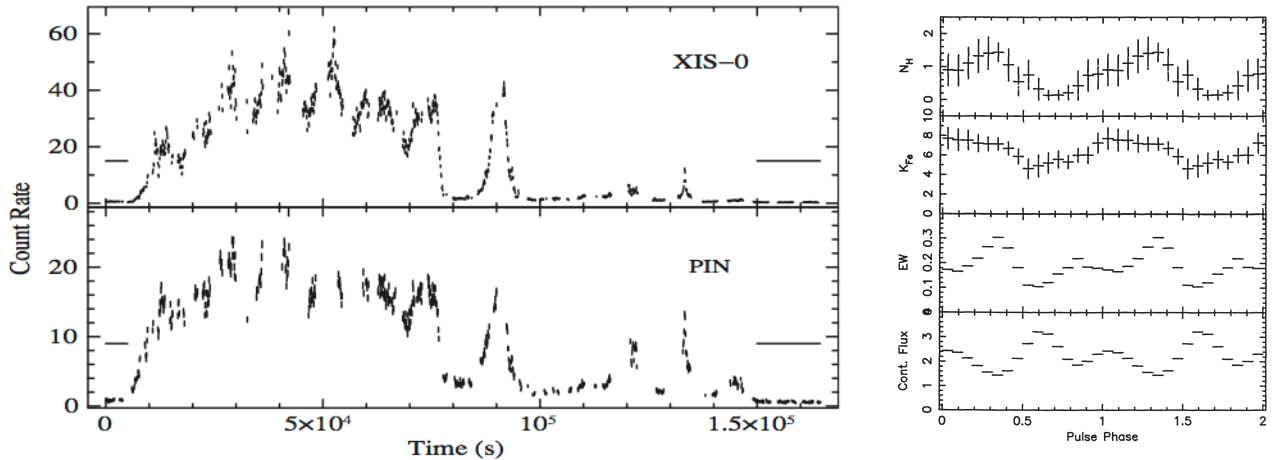


Figure: One orbit *Suzaku* light curve of Cen X-3 (left; Naik et al., 2011) and iron intensity modulation as a function of pulse phase (right; Day et al. 1993).

Previous observations:

- Iron K emission lines from near-neutral (fluorescence, ~6.4 keV, Fe I,II), He-like (~6.7 keV, Fe XXV), and H- like (6.95 keV, Fe XXVI).
- Observations during eclipse transitions show shallower eclipse for He-like vs. fluorescence.
 - Fluorescence region is more compact (Alfven shell? Or accretion disk?).
- Pulsations have been observed at low resolution (i.e. all lines summed)
 - Must be only the fluorescence line since extended

From Chandra HETG: Iron line has 3 components

- 6.399 ± 0.006 keV with EW=59.5 eV
 - consistent with Fe I-III at rest (Palmeri et al. 2003, A&A 410, 359)
- 6.656 ± 0.010 keV with EW=31.3 eV
 - consistent with Fe XXV $1s^2 {}^1S - 1s2p^3 P^0$ likely recombination
- 6.954 ± 0.008 keV (EW=15.9 eV) (Wojdowski et al. 2003)
 - consistent with Fe XXVI Ly α (see NIST)

Modeling the line:

- Fluorescence line fits with $\log \xi < 1$ photoionization model. From fitting get emission measure $n^2 V = 10^{41} \text{ cm}^{-3}$
 - Gas is clumped, not smooth
- H- and He-like lines fit with $\log \xi = 3.2$ photoionization model, $n^2 V = 10^{39} \text{ cm}^{-3}$

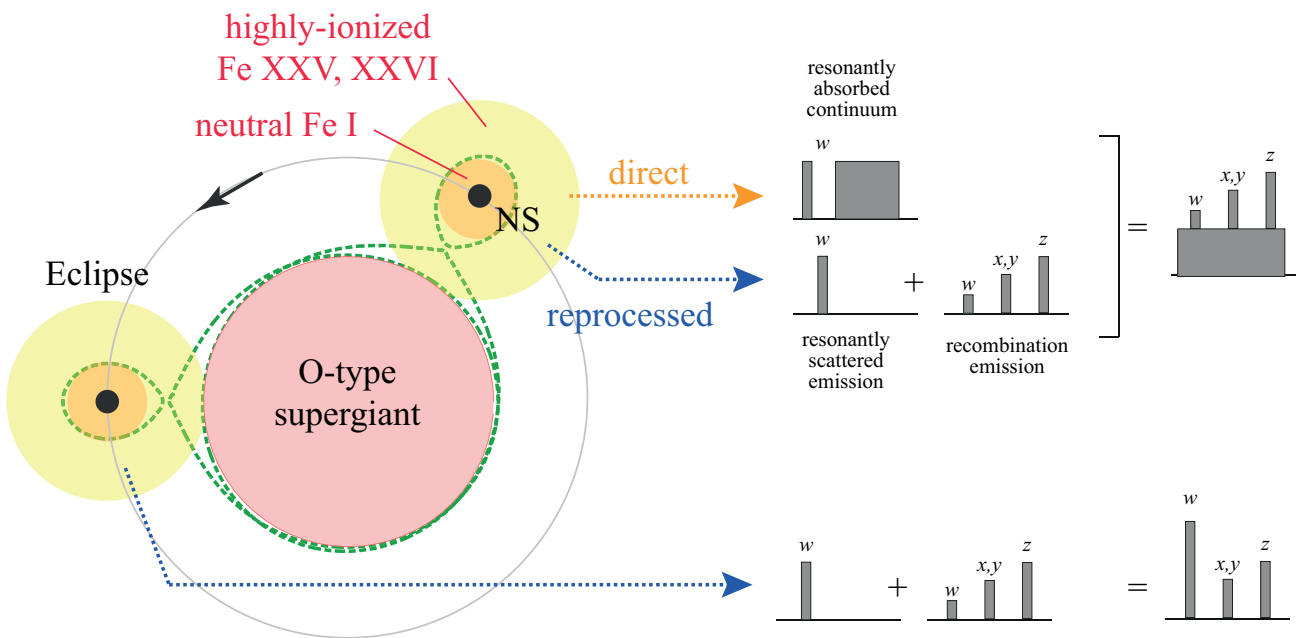


Figure: Schematic illustration of Cen X-3 (modified from Wojdowski et al., 2003).

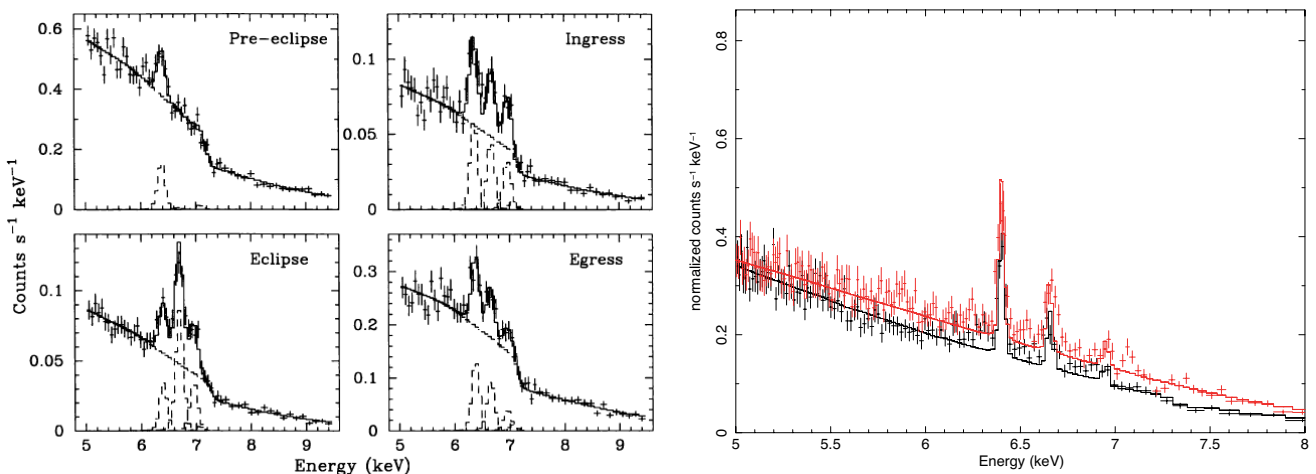


Figure: ASCA (Ebisawa et al., 1996) and Chandra (see, e.g., Iaria et al., 2005)

Question for ASTRO-H: What are the abundances of other ion peak elements? Can we learn about Alfvén shell from fluorescence line structure? Does fluorescence line pulse?

written by TK, TE

Further reading...

1. Day, C., S., R., et al. 1993, APJ, 408, 656 [[ADS](#)]
2. Ebisawa, K., et al. 1996, PASJ, 48, 425 [[ADS](#)]
3. Wojdowski, P., S. et al. 2003, ApJ, 582, 959 [[ADS](#)]
4. Iaria, R. et al. 2005, ApJ, 634, L161 [[ADS](#)]
5. Naik, S., et al. 2011, ApJ, 737, 79 [[ADS](#)]

Useful collection of conference/meeting

- International Astronomical Consortium for High Energy Calibration (IACHEC) [[link](#)]
- MSSL Workshop proceedings High-resolution X-ray spectroscopy with Chandra and XMM-Newton [[link](#)]
 - Behar et al., "X-ray spectroscopy and atomic data" [[link](#)]
 - Kahn et al., "Astrophysical X-ray spectroscopy" [[link](#)]
 - Kinkhabwala et al., "XSPEC model PHOTOION" [[link](#)]
- SXS spectral analysis meeting at University of Maryland in 2013
 - Paerels, "Lessons learned from analysis of XMM-Newton/RGS spectra" [[link](#)]
 - Reynolds, "Lessons learned from analysis Chandra grating spectra" [[link](#)]
 - Smith, "Atomic data : What do we have? What do we need?" [[link](#)]
 - Kaastra & Smith, "AtomDB vs. SPEX" [[link](#)]
 - Echart, "SXS subtleties learned from analysis of calibration data" [[link](#)]
 - Arnaud, "The future of XSPEC" [[link](#)]
 - Kaastra, "Capabilities and limitations of fitting codes" [[link](#)]
 - Kallman, "Capabilities and limitations of photoionization codes" [[link](#)]
 - Paerels, "How I would like to analyze SXS data" [[link](#)]
 - Mushotzky, "How I would like to analyze SXS data" [[link](#)]
 - Markevitch, "How I would like to analyze SXS data" [[link](#)]
- 1st ASTRO-H Summer School
 - Paerels, "Radiation processes" [[link](#)],
 - "Triplet and other processes" [[link](#)]
 - Kaastra, "Thermal radiation processes" [[link](#)],
 - "X-ray absorption" [[link](#)],
 - "Dust and DEMS" [[link](#)]
 - Smith, "Non-thermal radiation processes" [[link](#)],
 - "Spectral modeling and analysis" [[link](#)]
- Other Important Presentations
 - Smith, "Plasma codes utilized in XSPEC" [[link](#)]
 - Porquet, "Plasma diagnostics focusing on the He-like ion" [[link](#)]

Further reading...

1. Kallman & Palmeri (2007)
2. Beiersdorfer 2003
3. Smith & Brickhouse 2014
4. Wargelin, Beiersdorfer and GV Brown 2008
5. PAradis and Bleeker "X-ray Spectroscopy in Astrophysics" 1997
6. Pradhan & Nahar "Atomic Astrophysics and Spectroscopy"
7. Herzberg, "Atomic Spectra and Atomic Structure"

Coffee break: Traveling to AKIHABARA

Akihabara, or Akiba, is now known as the central place for Japanese geeks, who are called “Otaku”. On the main street of Akihabara, there are a lot of anime, manga, video game shops and their huge signboards.



You can also see girls who wear maid-like uniforms and are distributing flyers. They are waitresses of “maid cafes” where waitresses serve dishes like maids or anime characters. There they will draw what you request on a rice omelet with tomato ketchup. (Please check the dessert in the left photo!)



On the other hand, Akihabara is also famous as a town of electronics shops. If you go to the off street, you can find many small shops of electronic parts, computers, radios, audio instruments and junk etc. Akihabara is very near the University of Tokyo and other universities. Thus some of Japanese ASTRO-H members might have come to Akihabara to buy some electric parts needed in laboratories urgently.

Revision History & Contribution

Revision history:

- 2014/02/18 start the project, assined from T. Ohashi and T. Takahashi at SM11
- 2014/03/20 meeting at UMD (RM, TE, and HN)
- 2014/07/10 presentation at the 12th ASTRO-H Science Meeting (TE, ver 0.12)
- 2014/09/05 meeting at TMU (TE, HN, AF, RS, GB, and JK, ver0.12)
- 2015/03/05 presentation at the 13 th ASTRO-H Science Meeting (HN,ver1.00?)
- 2015/05/25 presentation at the Japanese-Dutch Bilateral WS (HN, ver1.00?)

Editors: Teruaki Enoto, Hirofumi Noda, Richard Mushotzky, and Timothy R. Kallman
Expert advisers and contributors: Adam Foster (AF, a chapter of Helium-like ion and physics of the treplet), Randall Smith (RS, a column on the X-ray Nomenclature), Maurice A. Letenegger (ML, charge exchange), Jelle Kaastra (JK, expert adviser), Gregory Brown (GB, expert adviser), Timothy R. Kallman (TK, the chapter of astrophysical plasma, astrophysical example Cen X-3), Elisa Costantini (EC, absorptiion, dust), Hirofumi Noda (HN, atmic processes and productions of summay figutes), and Teruaki Enoto (TE, H- and He-like ion, and astrophysical plasma).

Contact Information:

Your comments and inputs to the cookbook are welcome. Please contact us if you have good material.

<Point of contact, Teru Enoto / AH Cookbook group teruaki_enoto@10.alumni.u-tokyo.ac.jp>

<Point of contact, Hirofumi Noda / AH Cookbook group hirofumi.noda@riken.jp>

